

Article

# Performance of a Radar Mosaic Quantitative Precipitation Estimation Algorithm Based on a New Data Quality Index for the Chinese Polarimetric Radars

Yang Zhang <sup>1,\*</sup>, Liping Liu <sup>1</sup> and Hao Wen <sup>2</sup>

<sup>1</sup> State Key Laboratory of Severe Weather, Chinese Academy of Meteorological Sciences, Beijing 100081, China; liulp@cma.gov.cn

<sup>2</sup> Meteorological Observation Centre, China Meteorological Administration, Beijing 100081, China; wenhao@cma.gov.cn

\* Correspondence: zhangyang\_cams@cma.gov.cn

Received: 9 September 2020; Accepted: 28 October 2020; Published: 30 October 2020

**Abstract:** The quality of radar data is crucial for its application. In particular, before radar mosaic and quantitative precipitation estimation (QPE) can be conducted, it is necessary to know the quality of polarimetric parameters. The parameters include the horizontal reflectivity factor,  $Z_H$ ; the differential reflectivity factor,  $Z_{DR}$ ; the specific differential phase,  $K_{DP}$ ; and the correlation coefficient,  $\rho_{HV}$ . A novel radar data quality index ( $RQI$ ) is specifically developed for the Chinese polarimetric radars. Not only the influences of partial beam blockages and bright band upon radar data quality, but also those of bright band correction performance, signal-to-noise ratio, and non-precipitation echoes are considered in the index.  $RQI$  can quantitatively describe the quality of various polarimetric parameters. A new radar mosaic QPE algorithm based on  $RQI$  is presented in this study, which can be used in different regions with the default values adjusted according to the characteristics of local radar.  $RQI$  in this algorithm is widely used for high-quality polarimetric radar data screening and mosaic data merging. Bright band correction is also performed to errors of polarimetric parameters caused by melting ice particles for warm seasons in this algorithm. This algorithm is validated by using nine rainfall events in Guangdong province, China. Major conclusions are as follows.  $Z_H$ ,  $Z_{DR}$ , and  $K_{DP}$  in bright band become closer to those under bright band after correction than before. However, the influence of  $K_{DP}$  correction upon QPE is not as good as that of  $Z_H$  and  $Z_{DR}$  correction in bright band. Only  $Z_H$  and  $Z_{DR}$  are used to estimate precipitation in the bright band affected area. The new mosaic QPE algorithm can improve QPE performances not only in the beam blocked areas and the bright band affected area, which are far from radars, but also in areas close to the two radars. The sensitivity tests show the new algorithm can perform well and stably for any type of precipitation occurred in warm seasons. This algorithm lays a foundation for regional polarimetric radar mosaic precipitation estimation in China.

**Keywords:** polarimetric radar mosaic; quantitative precipitation estimation; bright band correction; radar data quality index

---

## 1. Introduction

For flash flood detection and warning, it is meaningful to obtain a large range of accurate quantitative precipitation estimation (QPE) products by using surface rain gauges and various remote sensing instruments. Radar has a number of advantages over other instruments, since it can

provide QPEs with a higher spatial and temporal resolution over a wide area within a relatively short period of time [1–3]. However, radars may face challenges over mountainous terrain due to radar partial beam blockages and range-dependent biases due to the increase in altitude with range [4]. Radar mosaic technology serves to mitigate these influences and improve radar QPE performances, since it can select or obtain the best-quality data from different radars.

The three-dimensional radar mosaic was developed using Weather Surveillance Radar 1988 Doppler radars to obtain three-dimensional radar mosaic data at a national or partial area scale in the conterminous United States beginning in 2005 [5]. Radar mosaic technology in this study differs from the three-dimensional radar mosaic. The three-dimensional radar mosaic produces constant altitude plan position indicator (CAPPI) data. Radar mosaic technology in this study aims to produce mosaic data used to estimate precipitation on the ground, so it usually employs a hybrid scan strategy to obtain high-quality data near the ground. Since the beginning, single-polarization radars have been used in such mosaics. The National Mosaic and Multi-Sensor QPE (NMQ) system of the USA was built upon the Collaborative Radar Acquisition Field Test data network with multiple single-polarization radars and sensors [6]. In this system, the hybrid scan reflectivity factors of single radar are obtained first. Then, the data are mosaicked to calculate QPE based on different  $Z$ - $R$  relationships ( $R$  is the rainfall rate and  $Z$  is the reflectivity factor) corresponding to five types of precipitation. They include stratiform, convective, and warm cloud precipitation, as well as hail and snow. Some studies have also used the radar mosaic QPE algorithm with single-polarization radars in China [7–10]. Although different methods are employed to improve radar data quality or rainfall estimators, all are similar to those in the NMQ system. Only  $Z_H$  is used to calculate precipitation.

As the weather radars are upgraded to polarimetry, it becomes possible to use various polarimetric parameters (e.g., the horizontal reflectivity factor  $Z_H$ , differential reflectivity factor  $Z_{DR}$ , specific differential phase  $K_{DP}$ , and correlation coefficient  $\rho_{HV}$ ) in mosaics and to estimate precipitation. However, in the Multi-Radar Multi-Sensor (MRMS) system developed based on the NMQ system [11],  $Z$ - $R$  relationships are used to calculate QPE at the first stage. The QPE algorithms of the MRMS system are largely based upon NMQ QPE components [11]. Recently, studies have focused on developing a seamless polarimetric synthetic QPE calculated via a combination of specific attenuation  $A$ ,  $K_{DP}$ , and  $Z_H$  within the MRMS system. This new polarimetric radar QPE algorithm applies  $R(A)$  in areas where radar is observing pure rain,  $R(K_{DP})$  in regions potentially containing hail, and  $R(Z_H)$  elsewhere [3]. Both systematic and random errors are reduced by using  $A$ ,  $K_{DP}$ , and  $Z_H$  (rather than only  $Z_H$ ) to calculate QPE. However, the QPE product still needs further refinements in very light and sporadic rain where the attenuation signal is too weak, and in widespread light stratiform rain [3]. The estimator  $R(A)$  must be very carefully used in the above situations or else local adjustment will be needed. However, the performance of  $R(A)$  is unstable for Guangzhou radar when estimating precipitation during rainfall events with hourly accumulations below 50 mm [12]. Hence, the other polarimetric parameters (e.g.,  $Z_H$ ,  $Z_{DR}$ , and  $K_{DP}$ ) are chosen to estimate precipitation in this study. Therefore, the use of  $Z_H$ ,  $Z_{DR}$ , and  $K_{DP}$  to obtain accurate mosaic QPE products is the main focus of this study.

The quality of radar data is crucial for radar mosaic and QPE techniques. The quality is affected by many factors, including partial beam blockages, bright band (BB), signal-to-noise ratio (SNR), and non-precipitation echoes. There have been many studies [13–16] on quality control methods for solving the problems caused by partial beam blockages, low SNR, and non-precipitation echoes, which are not studied here. When estimating QPE, BB should be paid attention to. As a phenomenon of echo enhancement due to the melting of ice particles, BB brings errors to QPE. It was subject to attention in the early days of radar meteorology [17–20]. The appearance of BB often leads to overestimation of precipitation in single-polarization radar. In order to mitigate these biases, many studies have focused upon the identification of BB [21,22] and the correction of data affected by BB effects [23,24]. For instance, Zhang and Qi [23] (hereafter ZQ10) developed a real-time VPR correction algorithm based on single-polarization Weather Surveillance Radar-1988 Doppler reflectivity and environmental data. These studies only focused on precipitation estimates using the

Z-R relationship. At the same time, the  $Z_{DR}$  in BB was also found to increase as the snow melted [25,26]. In the study of Mario et al.,  $Z_{DR}$  and  $K_{DP}$  are found to sharply increase just above the freezing level and below it [27]. The vertical variations of  $Z_{DR}$  and  $K_{DP}$  in BB can cause more uncertainties in QPE; however, most studies do not take this into account when estimating precipitation. Therefore, they are considered in this study to improve the radar QPE performance.

Besides the data quality control, data quality quantification is also very important. The data quality quantification index can describe the data quality quantitatively. Friedrich et al. developed a quality index algorithms detect and quantify the influence of many factors upon radar data. The factors include beam broadening, the height of the first radar echo, ground clutter contamination, return from non-weather-related objects, and attenuation of electromagnetic energy by hydrometeors [28]. In their study, the index fields are made based on the C-band polarimetric radar in southern Germany, but they are not used for further processing. In fact, this similar index is very useful for radar data application. Vulpiani et al. proposed a quality map  $Q$ , which is a kind of quality quantification index. It is subjectively generated by combining the quality indicators: static-clutter map, radial velocity, texture of  $Z_{DR}$ ,  $\rho_{HV}$ , and  $\Phi_{DP}$ . They use it to discriminate the nonmeteorological targets from weather returns [29]. This application is used for two C-band polarimetric radars in the mountainous areas of Italy and achieves encouraging results. It indicates that this quality index shows advantages of the application of the radar located in complex terrain. This characteristic of the quality index is very important in radar mosaic. Therefore, the quality index is also the core technical parameter in radar mosaic, especially when radars are located in the mountainous area. In French and American radar mosaic systems, these similar quality indexes are well used [30,31]. The quality indexes of the French system are used as weights to obtain the best rainfall estimation. They only depend upon the presence of ground clutter, the degree of blocking, and the altitude. The quality indexes of the American system (MRMS system) are used to choose high-quality  $Z_H$  [31]. Only partial beam blockage and BB are considered in their quality index. Although all these above quality indexes are well used in different radars or radar systems, they still need to be improved, especially for the Chinese polarimetric radars. The influences of SNR upon radar data quality are not considered in their study, but SNR has obvious influence in data quality, especially for  $Z_{DR}$ ,  $K_{DP}$ , and  $\rho_{HV}$  of Chinese polarimetric radars [16,32]. Besides this, the BB correction performance influences the data quality after the correction is applied to these data. If this factor is not considered, the corrected data cannot be used in a correct way. Therefore, a new radar data quality index (RQI) must be proposed to accurately represent the quality of  $Z_H$ ,  $Z_{DR}$ ,  $K_{DP}$ , and  $\rho_{HV}$  of the Chinese polarimetric radars. This is a novel and core radar mosaic technical parameter that is proposed in this study.

Recently, there has been a trend of upgrading radars to use polarimetry in China. Since quality varies among radars, the problem of how to combine them effectively to obtain the mosaic data and accurate QPE is very significant. The aim of this study is to develop and validate a suitable polarimetric radar mosaic QPE algorithm, so as to lay a foundation for regional polarimetric radar mosaic precipitation estimation in China. It should be noted that this algorithm is for near real-time operational use. For this purpose, the two S-band operational polarimetric radars separately located in Guangzhou and Yangjiang are used in this study. Nine rainfall events in Guangdong, China, are used to validate the proposed radar mosaic algorithm. Section 2 describes the data used in this study, as well as the details of the polarimetric radar mosaic QPE algorithm. Section 3 presents the performances of the radar mosaic QPE algorithm and analyzes its advantages for QPE. Some discussions are presented in Section 4, and Section 5 presents the conclusions.

## 2. Materials and Methods

### 2.1. Polarimetric Radar Data Analysis

Guangzhou and Yangjiang S-band polarimetric radars are used in this study to explore a new polarimetric radar mosaic QPE algorithm. The quality and consistency of the two radars' data need

to be studied before the mosaic is constructed. It makes sense to construct the mosaic only if the data from the two radars are consistent in the common-coverage area.

### 2.1.1. Beam Blockage Situation of Polarimetric Radars

Guangdong province is dominated by mountains. Its terrain is shown in Figure 1a. The positions of the Guangzhou and Yangjiang radars are shown in Figure 1a,b with black triangles. The beam blockages of the two radars are calculated with the method described by Bech et al. [33], and they are shown in Figure 2. The Guangzhou radar is located in the plain area, and the beams are only slightly blocked (Figure 2a). However, there are many mountains around the Yangjiang radar, and the beams are severely blocked at many azimuthal angles (Figure 2b). The blockages are obvious at many northern azimuthal angles, as well as some eastern and western ones. The highest beam blockage percentage nearly reaches 100%, and Yangjiang radar almost obtains no effective echoes in those azimuthal angles. The blockages are topped at  $2.4^\circ$  tilt of Yangjiang radar at some northern azimuthal angles, which are shown in Figure 2d. If only Yangjiang radar data were utilized to estimate precipitation, there would be obvious underestimation or even no QPE value in some beam blockage regions.

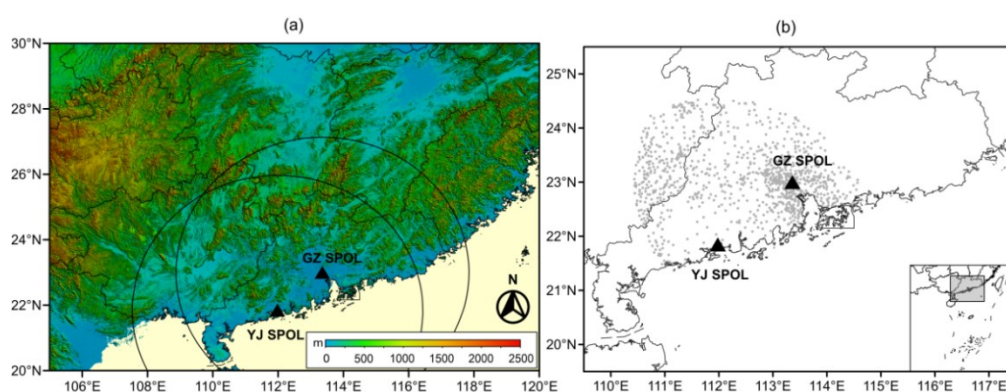


**Figure 1.** Distributions of the Guangzhou and Yangjiang S-band polarimetric radar (GZ SPOL, and YJ SPOL, black triangles) in (a,b), and the gauge stations (gray circles) in (b). The background color in (a) indicates altitude, and the black circles (460-km radius) indicate the maximum range of radar observations. The gauge stations are less than 300 km from either radar in (b). The gray rectangle in the lower right of (b) shows the extent of the region in South China.

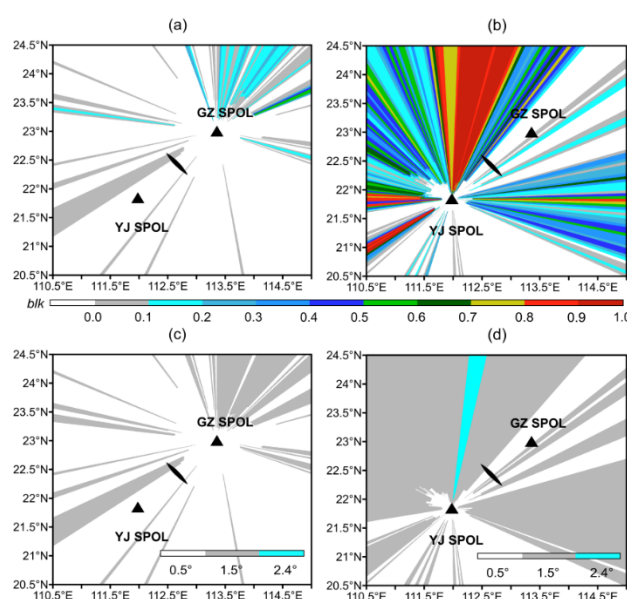


**Figure 2.** Beam blockages at  $0.5^\circ$  tilt of (a) Guangzhou radar and (b) Yangjiang radar. The triangles indicate radars and the narrow black area between the two radars indicates the common area for

comparing data. The blockages are topped at the elevation angles of Guangzhou radar and Yangjiang radar which are shown in (c,d), respectively.

### 2.1.2. Data and Quality Control Method

S-band single-polarization radars in Guangdong province were upgraded to polarimetric radars in 2016. After the radars were upgraded, the range bin length became 0.25 km, but the scan period remained 6 min. The main specifications are shown in Table 1.

**Table 1.** Main specifications of the S-band polarimetric radar.

Parameter Type	Setting
The antenna diameter (m)	8.54
The antenna gain (dB)	45.31
The beam width (°)	<0.98
The first side lobe (dB)	<−30
The wave length (cm)	10.3
The operating mode	simultaneous horizontal and vertical transmission and reception
The minimum detectable power (dBm)	−117.8
The volume scan mode	VCP21 (9 tilts)
The range resolution (km)	0.25

Meanwhile, a series of tests were conducted for the transmitter and the receiver. The difference between the expected value and the measured value of the radar constant is calculated based on the radar transmit power and the radar equation, and the difference is corrected in real time. The transmitter is calibrated in this way. The receiver is calibrated with built-in testing and sun-calibration method. These tests indicated that  $Z_H$  accuracy is better than 1 dB, meeting the requirements for QPE.  $Z_{DR}$  is also calibrated with vertical pointed calibration method before the radar operation.

A quality control procedure must be applied to polarimetric radar data before radar mosaic construction and precipitation estimation. Firstly,  $Z_{DR}$  is smoothly filtered along the radial direction to reduce random fluctuations. The smoothing range bin number  $M$  depends upon the  $Z_H$  value. The value of  $M$  is as follows:

$$M = \begin{cases} 3 & Z_H \geq 45\text{dBZ} \\ 5 & 35\text{dBZ} \leq Z_H < 45\text{dBZ} \\ 7 & Z_H < 35\text{dBZ} \end{cases} \quad (1)$$

Three, five, or seven gates are used in a running average for  $Z_{DR}$  based on  $Z_H$  values. In this way,  $Z_{DR}$  is smoothed to various degrees with various reflectivity factors to avoid non-complete smoothing for weak echoes and excessive smoothing for strong ones.

Kalman filtering is used for  $\Phi_{DP}$ , and  $K_{DP}$  is calculated by a linear least squares fit using  $N$  samples of the  $\Phi_{DP}$  [14].  $N$  is the number of consecutive radar bins for the piecewise linear fit, which is adjusted according to three reflectivity factor levels:

$$N = \begin{cases} 9 & Z_H \geq 45\text{dBZ} \\ 13 & 35\text{dBZ} \leq Z_H < 45\text{dBZ} \\ 17 & Z_H < 35\text{dBZ} \end{cases} \quad (2)$$

This adaptive adjustment is intended to follow steep phase changes in intensive precipitation regions while maintaining a low variation in the estimated  $K_{DP}$  in light precipitation regions [13]. Since the range resolution of the radar is 0.25 km, the estimation can tolerate small-scale variability up to 2.25 km under heavy rain and large-scale variability up to 4.25 km under light rain. Moreover,  $K_{DP}$  is also smoothly filtered in the same way as  $Z_{DR}$  to reduce random fluctuations. Besides this, the data influenced by radio frequency interference have been identified and eliminated with the method proposed by Wen et al. [34].

During May to June 2016, nine rainfall events were observed by the two radars and the rain gauges around them (Table 2). The rain gauge stations in Figure 1b are all less than 300 km from either radar. Gauges used in this study are tipping bucket rain gauges. The resolution of the rain gauge data is 0.1mm, and the data are received every one minute. In this study, the data from these gauges are accumulated in an hour separately to evaluate the QPE performances. The gauge data are also quality controlled with method proposed by Gou et al. [9]. The quality control for gauge data is mainly carried out by comparing the spatial consistency of gauge data. In general, the rainfall data of gauge stations should not be very different from that of several nearby stations. Once it exceeds a certain range, the rainfall data of this gauge station is considered abnormal and this isolated extreme data needs to be removed.

**Table 2.** A list of the nine rainfall events used in this study.

#	Date (UTC)	Total Time (h)	No. of Valued Gauges	Mean Gauge Accumulation (mm)	Max Gauge Accumulation (mm)	Precipitation Type
1	6 May 2016	12	730	19.04	118.5	squall line
2	9–10 May 2016	34	905	34.68	222.8	convective
3	15 May 2016	10	963	14.19	67.1	squall line
4	19–21 May 2016	43	1001	55.77	416.6	stratocumulus
5	27–28 May 2016	24	991	30.48	177.2	squall line
6	4–5 June 2016	24	935	29.20	109.4	stratocumulus
7	9 June 2016	8	269	9.56	80.2	stratocumulus
8	11–14 June 2016	86	1007	44.57	211.4	stratocumulus
9	15 June 2016	6	719	11.99	79	squall line

### 2.1.3. Analysis of Polarimetric Radars Data Consistency

The radars' data consistency needs to be confirmed prior to construction of the radar mosaic. To minimize the influence of partial beam blockages, only the narrow black region between the Guangzhou and Yangjiang radars (Figure 2) is selected as a common area for radars data comparison. This region falls within 100 km of the two radars. Rainfall events listed in Table 2 occurring in Guangdong Province are selected for data comparison. Despite the small size of the selected area, extensive data are available for effective comparison.

After the quality control procedure is applied to the two radars' data, the consistency between them is analyzed. The two radars' CAPPI (2 km) data are collected for comparison, and the frequency distributions of  $Z_H$ ,  $Z_{DR}$ , and  $K_{DP}$  are shown in Figure 3. The diagonal lines are equal lines. It is apparent that the three polarimetric parameters are basically distributed near the diagonal lines. The average differences are 0.2555 dB ( $Z_H$ ), 0.0061 dB ( $Z_{DR}$ ), and 0.0058 °/km ( $K_{DP}$ ), respectively. The standard deviations of the differences are 4.4848 dB ( $Z_H$ ), 0.3527 dB ( $Z_{DR}$ ), and 0.2380 °/km ( $K_{DP}$ ), respectively. Considering that there are biases caused when calculating CAPPI (2 km), the two radars' data are basically consistent, which satisfies the mosaic condition.

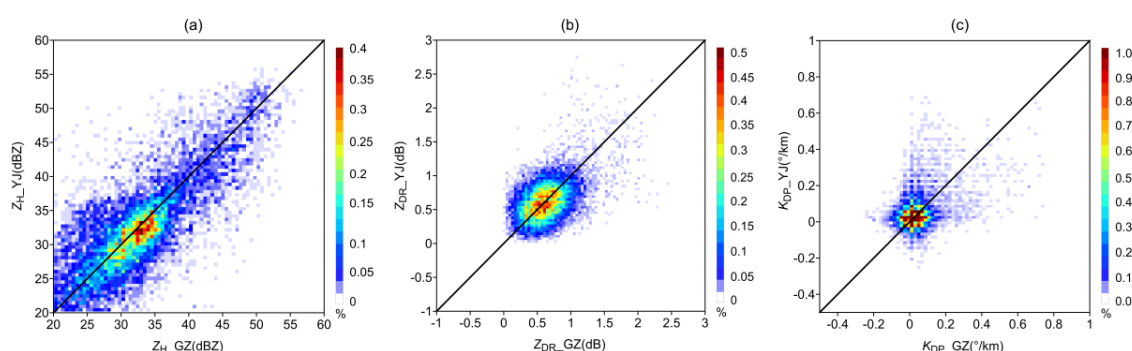


**Figure 3.** Frequency distributions of (a)  $Z_H$ , (b)  $Z_{DR}$ , and (c)  $K_{DP}$  from 2 km CAPPI. The horizontal axis indicates Guangzhou radar data and the vertical axis indicates Yangjiang radar data.

## 2.2. The Key Methods in Polarimetric Radar Mosaic QPE Algorithm

In the polarimetric radar mosaic QPE algorithm, precipitation is estimated with the mosaic hybrid scan data. It should be noted that the main purpose of the radar data mosaic in this study is to estimate precipitation. The hybrid scan mosaic algorithm used in this study differs from that of the three-dimensional mosaic. The details of the polarimetric radar mosaic QPE algorithm are described below.

### 2.2.1. BB Correction

When data from different radars are mosaicked in a grid, the heights of the data are different. Some of them may be in the melting layer. Their data quality is obviously influenced by BB. Therefore, BB correction is necessary in the radar mosaic QPE algorithm.

BB is caused by the melting ice particles; it affects polarimetric radar data, leading to an increase in  $Z_H$ ,  $Z_{DR}$ , and  $K_{DP}$ , and a decrease in  $\rho_{HV}$  [25,26]. These changes can make QPE performances uncertain. It is necessary to correct these changing data; however, most previous studies have only corrected  $Z_H$  to improve QPE performance. In fact, there are some other relations between polarimetric parameters and rain rate  $R$  for estimating precipitation in the polarimetric radar QPE algorithm. Besides  $Z_H$ , some other radar data (such as  $Z_{DR}$  and  $K_{DP}$ ) also need to be corrected. Although  $\rho_{HV}$  is not directly used to calculate precipitation, it is very sensitive to mixed-phase precipitation particles and can be used to detect BB height. For BB correction, convective and stratiform precipitation echoes are first segregated, then the BB height range is identified, and finally the data are corrected after the vertical profile model is established.

#### (a) Convective and stratiform precipitation segregation

The composite reflectivity factor ( $CR$ ) and vertically integrated liquid water content ( $VIL$ ) are chosen to segregate the convective and stratiform precipitation. Convective precipitation is identified based on that  $CR > 50$  dBZ or  $VIL > 6.5$  kgm<sup>-2</sup> [23,35]. Otherwise, the precipitation is classified as being stratiform.

#### (b) BB height range identification

Once the precipitation type is determined, the following steps are performed only for stratiform precipitation. The apparent vertical profile of data (AVPD) is obtained according to the stratiform precipitation data. The word “apparent” indicates the beam broadening effects in the vertical profile. When a radar observes echoes at a long distance, the height of the vertical profile will be increased due to beam broadening. Therefore, it should be noted that the obtained BB top height will be higher than the “truth”; however, since the statistics and correction of the data are both affected by beam broadening, the data correction is reasonable as long as the data at BB bottom height are correct. This method has been verified for  $Z_H$  correction in several studies [23,24].

Since  $Z_{DR}$ ,  $K_{DP}$ , and  $\rho_{HV}$  are unreliable when  $SNR$  of the polarimetric radars in Guangdong is below 20 dB [16,32], AVPDs are collected via the ZQ10 method [23] used for  $Z_H$  with the added condition that the data collected here must have an  $SNR > 20$  dB to ensure high-quality. The AVPD frequency distributions of  $Z_H$ ,  $Z_{DR}$ ,  $K_{DP}$ , and  $\rho_{HV}$  (shown in Figure 4) are obtained from the Guangzhou and Yangjiang radar data according to the nine rainfall events listed in Table 2. High frequencies indicate that data are concentrated, and show the same feature of most profiles. AVPDs of  $Z_H$  and  $Z_{DR}$  have the same obvious BB feature: the frequencies are very high in the peak-value region, meaning that a large number of data affected by BB become larger than the data near the ground. The same feature provides the basis for the AVPD model. Although the AVPDs of  $K_{DP}$  also show that data affected by BB become larger than data near the ground, data points in the peak-value region are more dispersed than those of  $Z_H$  and  $Z_{DR}$ , which poses a challenge for  $K_{DP}$  correction in BB. There is a strange profile in the high altitude of the  $\rho_{HV}$  AVPDs because  $\rho_{HV}$  does not go back close to unity in ice. There are two possible reasons for the strange profile of  $\rho_{HV}$  in the high altitude. One reason is the ice mixed with rain. The other one is the  $SNR$  with too small value. The reflectivity of the ice in the high altitude is small, and its  $SNR$  is also small. The  $SNR$  has an



obvious influence on  $\rho_{HV}$  of the polarimetric radars in Guangdong. When the  $SNR$  becomes small, the quality of  $\rho_{HV}$  becomes bad [16,32]. Although only data corresponding to  $SNR > 20$  dB are collected to obtain AVPD of  $\rho_{HV}$ , the  $SNR$  of the ice in the high altitude is smaller than that in the low altitude, and may be close to 20 dB. Therefore, it is the small  $SNR$  that makes the  $\rho_{HV}$  profile strange in the high altitude where pure ice exists.

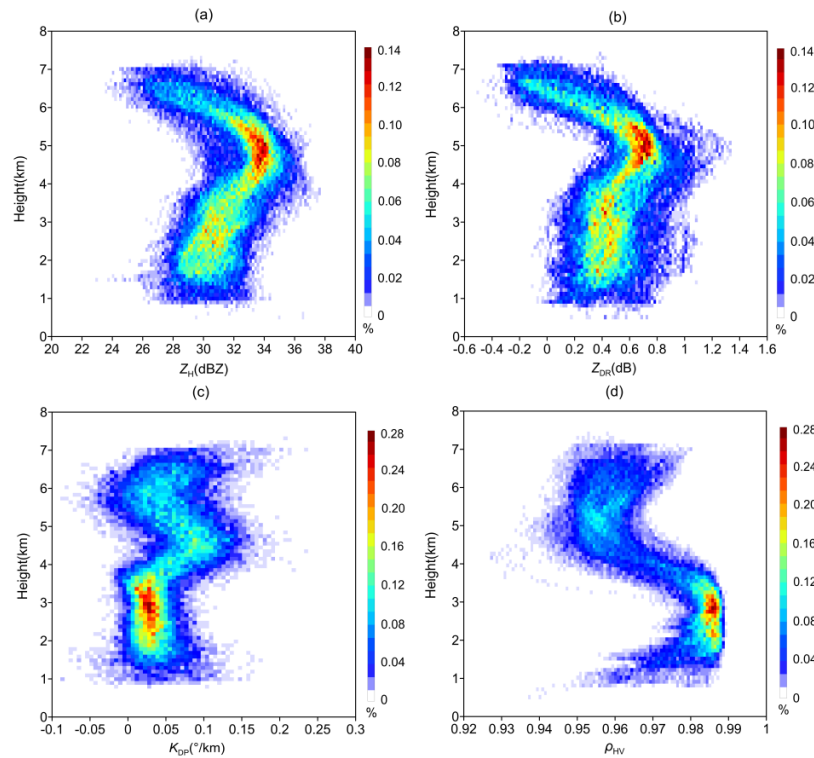


**Figure 4.** Apparent vertical profile of data (AVPD) frequency distributions of (a)  $Z_H$ , (b)  $Z_{DR}$ , (c)  $K_{DP}$ , and (d)  $\rho_{HV}$  derived from the nine rainfall events during May to June 2016.

An ideal AVPD model for  $Z_H$ ,  $Z_{DR}$ , and  $K_{DP}$  is established based on the same feature of frequency distributions, and it is shown in Figure 5. It can represent most AVPDs of  $Z_H$ ,  $Z_{DR}$ , and  $K_{DP}$ . The main height parameters include BB top height ( $h_t$ ), BB bottom height ( $h_b$ ), and BB peak height ( $h_p$ ).

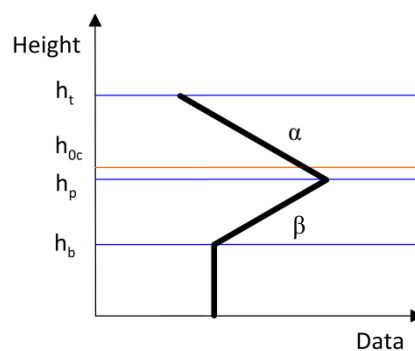


**Figure 5.** The ideal AVPD model of  $Z_H$ ,  $Z_{DR}$ , and  $K_{DP}$ .  $h_t$  indicates the bright band (BB) top height,  $h_b$  indicates the BB bottom height,  $h_p$  indicates the BB peak height, and  $h_{0c}$  indicates the 0 °C height.  $\alpha$  and  $\beta$  indicate the respective slopes of the two lines.

The main height parameters must first be identified to obtain the ideal AVPD model. The height of 0°C is read from the sounding data, and the BB peak in AVPD is obtained by searching the



maximum value of data around the 0 °C height. The BB top is obtained by searching the first inflection point above the BB peak in AVPD.

It is very important to identify the BB bottom height, because the correction factor is calculated with reference to  $h_b$ . However, the bottom data of  $Z_H$ ,  $Z_{DR}$ , and  $K_{DP}$  are scattered, while the bottom data of  $\rho_{HV}$  are very concentrated (see Figure 4). Most bottom  $\rho_{HV}$  data are concentrated above 0.975, which is helpful for identifying  $h_b$ . Therefore, the method used in the MRMS system that identifies  $h_b$  by searching for the first inflection point of  $Z_H$  is not used in this study [23,24]. Instead,  $\rho_{HV}$  is used to identify  $h_b$ .  $\rho_{HV}$  is searched from  $h_p$  down; when the value change rate of  $\rho_{HV}$  is approximately zero, its height is  $h_b$ , meaning that  $\rho_{HV}$  is basically stable. When  $\rho_{HV}$  is stable, the phase of the hydrometeors is basically unchanged. What's more, it should be noted that most precipitation particles at the BB bottom height are liquid particles, so  $\rho_{HV}$  must be larger than a threshold value, which is set to 0.975 in this study. A similar method proposed by Qi et al. [36] that uses  $\rho_{HV}$  to detect  $h_b$  proves to perform better than that using  $Z_H$  (such as ZQ10) on tests for three heavy precipitation events from different geographical regions and seasons in the United States, which indicates the feasibility of the proposed method in this study.

### (c) AVPD modeling and BB correction

The height parameters,  $h_t$ ,  $h_b$ , and  $h_p$ , are used to derive a parameterized, two-piece-linear AVPD model. One piece is between the BB top and the peak and another is between the BB bottom and the peak. The slope values  $\alpha$  and  $\beta$  are fitted using two data sections according to a least squares method. The correction factor  $D_a(h)$  is obtained based on the established AVPD model, which is shown as follows:

$$D_a(h) = \begin{cases} \alpha[h(r) - h_p] + \beta[h_p - h_b] & h_p < h(r) \leq h_t \\ \beta[h(r) - h_b] & h(r) \leq h_p \end{cases} \quad (3)$$

The corresponding data are corrected as follows:

$$D_c(\varphi, 0) = D_o(\varphi, h) - D_a(h) \quad (\varphi, h) \in BBA, \quad (4)$$

where  $r$ ,  $\varphi$ , and  $h$  are the range, azimuth, and height of the beam axis at a given gate, respectively.  $D_o(\varphi, h)$  and  $D_c(\varphi, 0)$  are the raw and corrected data, respectively. In this study, these data include  $Z_H$  (dBZ),  $Z_{DR}$  (dB), and  $K_{DP}$  (°/km).

In the real time applications, these three steps are implemented for one radar volume scan data to obtain its AVPD model at every volume scan period. The parameters of the AVPD model adapt with time, and the BB correction is applied in real time. It should be noted that the AVPD model is only derived and applied to the BB affected area (BBA) rather than to the whole radar coverage.

The above method is based on a specific set of data. They are from the rainfall events occurred in the warm season of Guangdong, China. The similar environment of these events makes AVPD relatively stable. This provides a guarantee for the effectiveness of this BB correction method, especially for warm season rainfall. Although AVPD changes due to microphysics and changing events, the parameters of the AVPD model adapt with time. These changing parameters can help mitigate correction biases due to the changing AVPD. However, when the environment changes largely, such as when a winter stratiform rain behind a cold front occurs, the ideal AVPD model shown in Figure 5 may be very different. This correction method may not be useful then. Further improvements can be made in the future studies. This BB correction method proposed in this study is better used for warm season rainfall for now.

### 2.2.2. Radar Data Quality Index and Polarimetric Radar Mosaic Algorithm

The hybrid scan data for the single radar need to be obtained before constructing the radar mosaic. The basic principle of the hybrid scan is to select the ground-clutter-free data to be as low as possible from the ground without obvious blockages. This differs from the three-dimensional mosaic, which aims to obtain data at different heights, such as CAPPI. In this study, data from the

lowest tilt with beam blockages of  $<0.3$  and  $\rho_{HV} > 0.7$  are chosen as the hybrid scan data based on this principle, to avoid complex terrain influences.

The hybrid scan data can be obtained with the above method and then used to construct the radar mosaic. Although BB correction has been applied to the data, it is still important to know the radar data quality. Only when the data quality is known quantitatively, high-quality data can be selected to obtain the high-quality mosaic data. Therefore, a radar data quality index ( $RQI$ ) is proposed in this study to quantitatively describe the data quality. It is referenced from a radar QPE quality index proposed by Zhang et al. [37] (hereafter Z11). Their index is proposed to identify and estimate the influences of partial beam blockage and BB upon QPE in their study. In fact, the QPE accuracy is mainly related to radar data quality and the relationship of radar parameters and rain rate. On the assumption that this relationship is accurate, radar data quality also can represent the accuracy of QPE. Therefore, in addition to representing data quality,  $RQI$  proposed in this study is expected to reflect QPE accuracy. This topic is also discussed in Section 4.2.

$RQI$  is governed by many factors, including partial beam blockages, BB, BB correction performance,  $SNR$ , and the non-precipitation echoes. BB correction performance and  $SNR$  are the factors not considered in other studies. However, these factors are important to the polarimetric parameters. The BB correction performance influences the data quality after the correction is applied to these data. If this factor is not considered, the corrected data cannot be used in a correct way in the BBA. Besides this, the qualities of Chinese polarimetric parameter  $Z_{DR}$ ,  $K_{DP}$ , and  $\rho_{HV}$  are obviously influenced by  $SNR$  [16,32]. Therefore,  $SNR$  is a key factor which need be considered when Chinese radar data are used. All the above factors are reflected in  $RQI$  with four indexes. They are introduced as follows.

$RQI_{blk}$  is an index proposed in Z11 study. It is still used here, shown as follows:

$$RQI_{blk} = \begin{cases} 1 & blk \leq 0.1 \\ \left(1 - \frac{blk-0.1}{0.4}\right) & 0.1 < blk \leq 0.5, \\ 0 & blk > 0.5 \end{cases} \quad (5)$$

where  $blk$  indicates the beam blockages. The influence of partial beam blockages upon radar data quality can be represented by  $blk$ .  $RQI_{blk}$  is the index affected by partial beam blockages and is calculated based on  $blk$ . At any given time, the quality of radar data is generally worse in complex terrains (large blockages) than in flatlands (no blockages). Therefore, when  $blk$  is large, the  $RQI_{blk}$  is set to small, and vice versa. The model of  $RQI_{blk}$  is shown in Figure 6a.

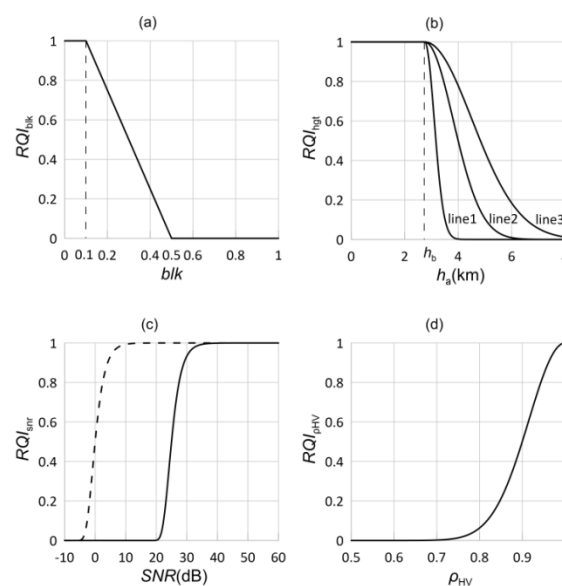


**Figure 6.** The models of (a)  $RQI_{blk}$ , (b)  $RQI_{hgt}$ , (c)  $RQI_{snr}$ , and (d)  $RQI_{\rho_{HV}}$ .  $h_b$  in (b) is the height of the BB bottom. Lines 1, 2, and 3 correspond to  $H_{sf}$  values of 500 m, 1500 m, and 2500 m, respectively. The  $SNR$  \*s (corresponding to  $snr$  \* s) of the dotted and solid lines in (c) are 0 dB and 25 dB, respectively.

$RQI_{\text{hgt}}$  is the other part of  $RQI$  in the Z11 study, and this index is affected by BB. However, in the Z11 study,  $RQI_{\text{hgt}}$  was calculated based on the assumptions that the thickness of BB is 700 m and that the data below  $h_{0c}$ -700 (m) are not affect by BB. This is obviously not accurate, so  $RQI_{\text{hgt}}$  is improved based on  $h_b$  according to the observed BB. In addition to the thickness of BB, a height scale factor is also a fixed value in the Z11 study, meaning that the BB correction performance is not considered. In this study,  $H_{\text{sf}}$  (m) is a height scale factor that changes with BB correction performance and is used in the new  $RQI_{\text{hgt}}$ . It is shown as follows:

$$RQI_{\text{hgt}} = \begin{cases} 1 & h_b > 0 \cap h_a < h_b \\ \exp\left(-\frac{(h_a - h_b)^2}{H_{\text{sf}}^2}\right) & h_b > 0 \cap h_a \geq h_b, \\ \exp\left(-\frac{h_a^2}{H_{\text{sf}}^2}\right) & h_b < 0 \end{cases} \quad (6)$$

$$H_{\text{sf}} = (2.5 - RND) \times 1000, \quad (7)$$

$$RND = \frac{|ND|}{ND_{\text{fix}}}, \quad (8)$$

$$ND = \frac{ave_{BB} - ave_{uBB}}{|ave_{uBB}|}, \quad (9)$$

where  $h_a$ (m) is the height of the beam axis,  $ave_{BB}$  is the average value of data in BB,  $ave_{uBB}$  is the average value of data under BB, and  $ND$  is the normalized difference between  $ave_{BB}$  and  $ave_{uBB}$ .  $ND$  represents data quality in BB. When  $ND$  is 0, the data in BB and under BB show good consistency. When  $ND$  is larger (resp. smaller) than 0, the average value of data in BB is larger (resp. smaller) than that under BB. The smaller the absolute value of  $ND$ , the better the BB correction performance is. The average value of data in BB and under BB are used to calculate  $ND$ , because it makes the calculation of  $RQI_{\text{hgt}}$  simple and feasible, and  $ND$  can basically reflect the performance of BB correction to make the  $RQI_{\text{hgt}}$  more reasonable. However, computing an average value under the BB will mask signature of microphysical processes that influence precipitation rate. In fact, some data under BB are not invariable, and have different changing trends. The changing trends of data under BB are discussed in Section 4.1.  $ND_{\text{fix}}$  is a fixed value of  $ND$ , which can stand for the average  $ND$  before BB correction. The default  $ND_{\text{fix}}$  of  $Z_H$  is 0.07, that of  $Z_{DR}$  is 0.5, and that of  $K_{DP}$  is 0.8. These are values derived from the nine rainfall events in this study. These values can be treated as the empirical values of radars in Guangdong. If the  $ND_{\text{fix}}$ s are used for other radars, the values of them can be adjusted according to the characteristics of local radar.  $RND$  is the ratio of  $|ND|$  and  $ND_{\text{fix}}$ , which can represent the BB correction performance. It is used to calculate  $H_{\text{sf}}$ . The equation of  $H_{\text{sf}}$  is established empirically to form the curves in Figure 6b.  $H_{\text{sf}}$  is limited in the range (500–2500) to avoid the abnormal value. The black lines 1, 2, and 3 in Figure 6b represent  $RQI_{\text{hgt}}$  with  $H_{\text{sf}}$  values of 500 m, 1500 m, and 2500 m, respectively.

The quality of radar data is generally worse in areas with low freezing levels than those with high freezing levels. The freezing levels are related to the height of the beam axis. Therefore,  $RQI_{\text{hgt}}$  is also influenced by the position of the beam axis relative to the BB bottom height,  $h_b$ . When the beam axis is below  $h_b$ , rain drops cannot be frozen and the value of  $RQI_{\text{hgt}}$  is 1; the higher the beam axis is relative to  $h_b$ , the less accurate that the data are. In addition, when the ambient temperature is too low,  $h_{0c}$  is very close to the ground and it is difficult to identify  $h_b$ , which is denoted by  $h_b < 0$  in formula (6), and only  $h_a$  is used to calculate  $RQI_{\text{hgt}}$ . The greater the height, the less accurate the data.

Z11 focused on the QPE of single-polarization radars, for which an  $RQI$  that only includes  $RQI_{\text{blk}}$  and  $RQI_{\text{hgt}}$  can satisfy requirements. However, radar data quality is also influenced by SNR and the non-precipitation echoes, especially for the polarimetric parameters  $Z_{DR}$ ,  $K_{DP}$ , and  $\rho_{HV}$ . SNR and the non-precipitation echoes are represented by  $snr$  (in linear scale) and  $\rho_{HV}$ , respectively. The index takes the form of a Gaussian function because it can represent the gradual change of radar data quality affected by  $snr$  or  $\rho_{HV}$ . The  $snr$  and  $\rho_{HV}$  are x-axis variables [38]. The value of the Gaussian function gradually decreases by controlling the threshold value.  $RQI_{\text{snr}}$  and  $RQI_{\text{PHV}}$  are shown as follows:

$$RQI_{\text{snr}} = \exp \left[ -0.69 \times \left( \frac{\text{snr}^*}{\text{snr}} \right)^2 \right], \quad (10)$$

$$RQI_{\rho_{\text{HV}}} = \begin{cases} 1 & \text{data: } Z_H, \rho_{\text{HV}} \\ \exp \left[ -0.69 \times \left( \frac{1-\rho_{\text{HV}}}{\Delta \rho_{\text{HV}}^*} \right)^2 \right] & \text{data: } Z_{\text{DR}}, K_{\text{DP}}' \end{cases} \quad (11)$$

where  $\text{snr}^*$  and  $\Delta \rho_{\text{HV}}^*$  are the threshold values of the Gaussian function. The  $\text{SNR}^*$  (corresponding to  $\text{snr}^*$ ) of  $Z_H$  is 0dB and those of  $Z_{\text{DR}}$ ,  $K_{\text{DP}}$ , and  $\rho_{\text{HV}}$  are 25 dB. The  $\Delta \rho_{\text{HV}}^*$  values of  $Z_{\text{DR}}$  and  $K_{\text{DP}}$  are 0.1.  $RQI_{\text{snr}}$  is the index affected by SNR, and is calculated based on  $\text{snr}$ . Some studies [16,32] have shown that when the SNR of the polarimetric radars in Guangdong falls below 20 dB,  $\rho_{\text{HV}}$ ,  $Z_{\text{DR}}$ , and  $K_{\text{DP}}$  become unreliable. Therefore, the index of  $RQI_{\text{snr}}$  is set to 0 when the SNR is below 20 dB, as can be seen from the model shown in Figure 6c.  $RQI_{\text{PHV}}$  is the index affected by the non-precipitation echoes, which is calculated based on  $\rho_{\text{HV}}$ . When precipitation echoes are mixed with the non-precipitation echoes,  $\rho_{\text{HV}}$  becomes smaller, and the qualities of the other polarimetric parameters become worse. When  $\rho_{\text{HV}}$  is under 0.7, the echoes are non-precipitation echoes [16], so the  $RQI_{\text{PHV}}$  of  $Z_{\text{DR}}$  and  $K_{\text{DP}}$  is set to 0. The  $RQI_{\text{PHV}}$  model of  $Z_{\text{DR}}$  and  $K_{\text{DP}}$  is shown in Figure 6d. Ground echo suppression has been made for  $Z_H$ , and echoes corresponding to low  $\rho_{\text{HV}}$  are treated in a certain way by the QPE algorithm, so the index of  $Z_H$  is set to 1.  $\rho_{\text{HV}}$  is the value reflecting non-precipitation echoes. Since it does not make sense to use  $\rho_{\text{HV}}$  to evaluate  $\rho_{\text{HV}}$ , the index of  $\rho_{\text{HV}}$  is also 1.

The simple linear and exponential functions are chosen to represent these indexes because of their computationally efficiencies for real-time implementation. All of the above indexes should be taken into account to quantitatively evaluate the polarimetric data quality;  $RQI$  is calculated as follows:

$$RQI = RQI_{\text{blk}} \times RQI_{\text{hgt}} \times RQI_{\text{snr}} \times RQI_{\rho_{\text{HV}}}. \quad (12)$$

Thus,  $RQI$  can represent the quality of radar data under the influence of partial beam blockages, BB, and BB performance, SNR, and non-precipitation echoes; thus, it can be used for data quality comparison. Based on this comparison, low quality data can be identified and eliminated. The polarimetric radar data mosaic algorithm flowchart is shown in Figure 7.

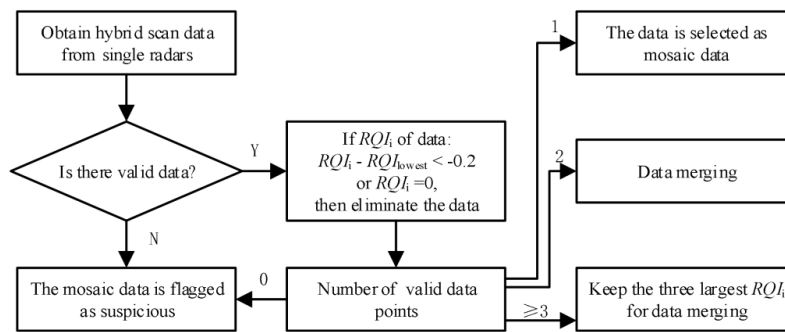


**Figure 7.** Flowchart describing the polarimetric radar data mosaic algorithm. The “data points” are original resolution polar data of different radars corresponding to the same ground grid.

The  $RQI$  of the lowest data ( $RQI_{\text{lowest}}$ ) is used as a standard value for comparison with the  $RQI$  of the other data in the same grid. The data point with an  $RQI$  value under  $RQI_{\text{lowest}} - 0.2$  or equal to 0 are treated as low quality data and eliminated. The number of the data points remaining determines how the mosaic data are obtained. If no data are left, the mosaic data of this grid would be flagged as suspicious. If only one data point is left, then this data point is selected to be the mosaic data for this grid. If there are two data points left, they are merged to obtain the mosaic data. For three or more data points left, only the three with the largest  $RQI$  values are merged.

Data merging is performed according to the following formula:

$$\text{Mosaic Data} = \frac{\sum_{i=1}^n w_L^i \times w_H^i \times RQI^i \times \text{Data}^i}{\sum_{i=1}^n w_L^i \times w_H^i \times RQI^i}, \quad (13)$$

$$w_L = \exp(-d^2/L^2), \quad (14)$$

$$w_H = \exp(-h^2/H^2), \quad (15)$$

where  $w_L$  and  $w_H$  are the horizontal and vertical weighting factors, respectively,  $d$  is the horizontal distance between the analysis point and the radar,  $h$  is the height of the radar bin, and  $L$  and  $H$  are the scaling factors with default values of 100 km and 2 km, respectively. *Mosaic Data* is the final mosaic radar data, and  $n$  is the mosaic radar number. In addition to the larger weighting given to the data that are closer to the ground and to the radar, the data with higher quality are also more heavily weighted in calculating the mosaic data, because *RQI* is considered as a weighting factor. This makes the mosaic data more reliable.

Although *RQI* is proposed for the Chinese radars in this study, it can be used in different regions and different seasons with different coverages. One thing that should be noted is that the default values of some variables need to be adjusted according to the characteristics of local radar.

### 2.2.3. Polarimetric Radar Mosaic QPE Algorithm

The mosaic data can be obtained based on the above algorithm. Firstly, the BB correction is applied to the polarimetric radar data, and then *RQI* is calculated and used to obtain the mosaic data. Finally, the mosaic data is used to estimate precipitation. The flowchart of this new QPE algorithm is shown in Figure 8.

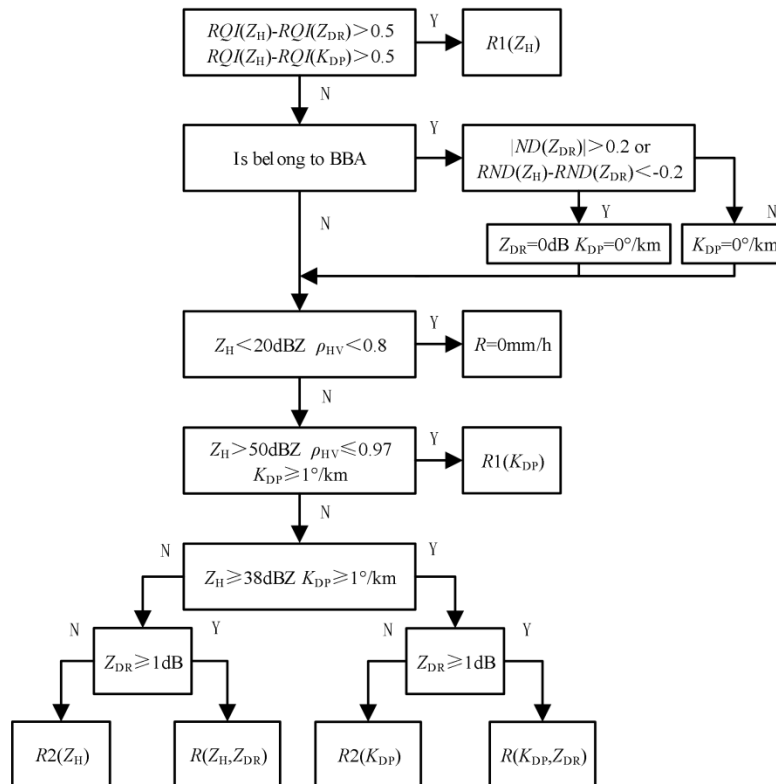


**Figure 8.** Flowchart describing the quantitative precipitation estimation (QPE) algorithm.

The QPE algorithm mainly follows the polarimetric radar QPE algorithm proposed by Zhang et al. [12] (hereafter Z18). The Z18 algorithm performs well for rainfall events occurring in Guangdong province; however, an  $SNR > 20$  dB is simply used to distinguish  $Z_{DR}$  and  $K_{DP}$  values of high quality from those of low quality in Z18 algorithm. The  $Z$ - $R$  relationship is used to estimate precipitation when  $Z_{DR}$  and  $K_{DP}$  have low quality. Although the same strategy is applied to the QPE

algorithm, the  $RQI$ s of  $Z_H$ ,  $Z_{DR}$ , and  $K_{DP}$  are used to determine whether the  $Z$ - $R$  relationship is suitable for estimating precipitation in the new QPE algorithm. This is because  $RQI$  can more accurately represent the quality of data than  $SNR$ . When  $RQI(Z_H) - RQI(Z_{DR}) > 0.5$  and  $RQI(Z_H) - RQI(K_{DP}) > 0.5$ , the quality of  $Z_H$  is much better than that of  $Z_{DR}$  and  $K_{DP}$ , thus the  $Z$ - $R$  relationship is used to estimate precipitation.

Data in BBA are different from data in other areas, and BB correction performances of different data are different. These all make estimating precipitation in the BBA more special. The QPE algorithm in the BBA needs to be different from the algorithm in the other areas, and it is studied here. Firstly, the influences of corrected  $Z_H$ ,  $Z_{DR}$ , and  $K_{DP}$  upon the QPE in the BBA are studied. In order to study these influences, average raw and corrected data in the BB are used to estimate precipitation, and precipitation estimated based on data at the BB bottom height is treated as the “truth” value to evaluate them. As statistical indicators of the QPE performance in this study, the correlation coefficient ( $CC$ ), root mean square error ( $RMSE$ ), normalized relative bias ( $NB$ ), normalized absolute error ( $NE$ ), and bias ratio of radar-estimated rainfall to the “truth” value of rainfall are obtained:

$$CC = \frac{\sum_{i=1}^n (QPE_i^{radar} - \overline{QPE_i^{radar}})(QPE_i^{truth} - \overline{QPE_i^{truth}})}{\sqrt{\sum_{i=1}^n (QPE_i^{radar} - \overline{QPE_i^{radar}})^2 \sum_{i=1}^n (QPE_i^{truth} - \overline{QPE_i^{truth}})^2}}, \quad (16)$$

$$RMSE = \sqrt{\frac{\sum_{i=1}^n (QPE_i^{radar} - \overline{QPE_i^{truth}})^2}{n}}, \quad (17)$$

$$NB = \frac{\sum_{i=1}^n (QPE_i^{radar} - \overline{QPE_i^{truth}})}{\sum_{i=1}^n QPE_i^{truth}} \times 100, \quad (18)$$

$$NE = \frac{\sum_{i=1}^n |QPE_i^{radar} - \overline{QPE_i^{truth}}|}{\sum_{i=1}^n QPE_i^{truth}} \times 100, \quad (19)$$

$$bias\ ratio = \frac{\sum_{i=1}^n QPE_i^{radar}}{\sum_{i=1}^n QPE_i^{truth}}, \quad (20)$$

where  $QPE$  is the rainfall derived from either radar or “truth” value, an overbar represents a mean value,  $n$  is the number of  $QPE_i^{truth} - QPE_i^{radar}$  pairs,  $RMSE$  has the same units as  $QPE$ , and  $NE$  and  $NB$  are both percentages. A *bias ratio* value larger (resp. smaller) than one indicates overestimation (resp. underestimation).

The evaluated statistical scores for radar QPE based on raw/corrected data in the BB are shown in Table 3. It is obvious that results derived from the corrected  $Z_H$  and  $Z_{DR}$  values are better than those derived from the corrected  $K_{DP}$  in terms of  $NE$  and  $NB$ . This indicates that the corrected  $Z_H$  and  $Z_{DR}$  values are more suitable for estimating precipitation in the BBA than the corrected  $K_{DP}$ . Therefore, only corrected  $Z_H$  and  $Z_{DR}$  are used to estimate precipitation in the BBA in this study.

**Table 3.** Evaluated statistical scores of radar QPE based on raw/corrected data in the BB. Radar QPE based on data at the BB bottom height is treated as the “truth” value.

Method	Based on Raw Data in BB			Based on Corrected Data in BB		
	CC	NE (%)	NB (%)	CC	NE (%)	NB (%)
$R1(Z_H)$	0.39	41.66	37.55	0.80	11.79	−1.24
$R2(Z_H)$	0.39	40.42	36.42	0.80	11.50	−1.22
$R1(K_{DP})$	0.15	100.2	73.30	0.26	60.28	16.96
$R2(K_{DP})$	0.15	97.52	71.14	0.26	59.02	16.41
$R(Z_H, Z_{DR})$	0.52	38.38	31.06	0.87	13.81	1.53
$R(K_{DP}, Z_{DR})$	0.16	93.39	66.61	0.26	59.30	16.17

It should be noted that BB correction cannot make data in BB equal to data under BB. The BB correction performance can be good or bad; when the  $Z_{DR}$  correction performance in BB is bad or

much worse than the  $Z_H$  correction performance in BB, the  $Z$ - $R$  relationship becomes the only choice for estimating precipitation. When  $|ND(Z_{DR})| > 0.2$ , the quality of  $Z_{DR}$  is considered to be very low, and the  $Z_{DR}$  correction performance in BB is bad. When  $RND(Z_H) - RND(Z_{DR}) < -0.2$ , the BB correction performance of  $Z_{DR}$  is considered to be much worse than that of  $Z_H$ . Therefore, when  $|ND(Z_{DR})| > 0.2$  or  $RND(Z_H) - RND(Z_{DR}) < -0.2$ , the  $Z$ - $R$  relationship is used in the QPE algorithm. These values used in this study are also empirical values, which can be adjusted according to the characteristics of local radar.

In addition,  $Z_H < 20$  dBZ and  $\rho_{HV} < 0.8$  are treated as the characteristics of the clear-air echo; there is no precipitation. The rest of the QPE algorithm flowchart follows the Z18 algorithm, which is not introduced in this study.

### 3. Results

#### 3.1. Performances of BB Correction

$ND$  can represent data quality in BB, so it can also reflect the data correction performance in BB. The  $ND$  frequencies of  $Z_H$ ,  $Z_{DR}$ , and  $K_{DP}$  derived from the nine rainfall events listed in Table 2 are shown in Figure 9; the gray histograms are derived from corrected data in BB, and those with black lines outside are derived from raw data in BB. The  $ND$ s of  $Z_H$ ,  $Z_{DR}$ , and  $K_{DP}$  all approach zero after BB correction, indicating good correction performance for the whole dataset. The average  $ND$ s of the corrected  $Z_H$ ,  $Z_{DR}$ , and  $K_{DP}$  values are 0.013,  $-0.026$ , and  $-0.241$ , respectively. The average  $ND$ s of  $Z_H$  and  $Z_{DR}$  are all much closer to zero than that of  $K_{DP}$ . The main  $ND$  frequency distributions of corrected  $Z_H$  and  $Z_{DR}$  are mostly Gaussian; however, that of the corrected  $K_{DP}$  is not. These all indicate that the BB correction performance of  $K_{DP}$  is not as good as that of  $Z_H$  and  $Z_{DR}$ . This is also why  $K_{DP}$  is not suitable for estimating precipitation in the BBA.

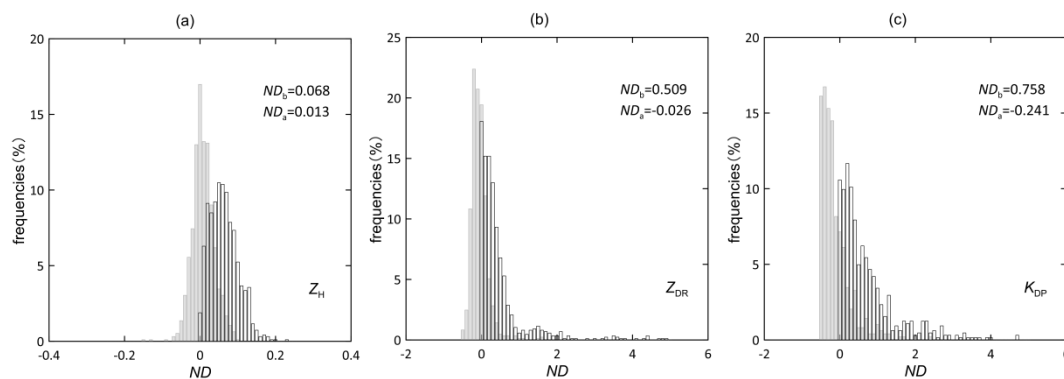


**Figure 9.**  $ND$  frequencies of (a)  $Z_H$ , (b)  $Z_{DR}$ , and (c)  $K_{DP}$  are shown with histograms. The gray ones are derived from corrected data, and those with black lines outside are derived from raw data in the BB.

Here we describe a case that reflects the BB correction performance of  $Z_H$ ,  $Z_{DR}$ , and  $K_{DP}$ . The original and corrected mosaic data at 20:54 on 15 June 2016 are shown in Figure 10. This is a squall line rainfall event. The small value of  $\rho_{HV}$  in the stratiform region behind the convective echoes of the squall line is obviously caused by BB, which is marked with a black circle in Figure 10a–h. Blue in Figure 10h represents BBA. Most of the BBA is in the black circle. The values of the corrected mosaic  $Z_H$ ,  $Z_{DR}$ , and  $K_{DP}$  in the circles have been reduced compared with the original data.



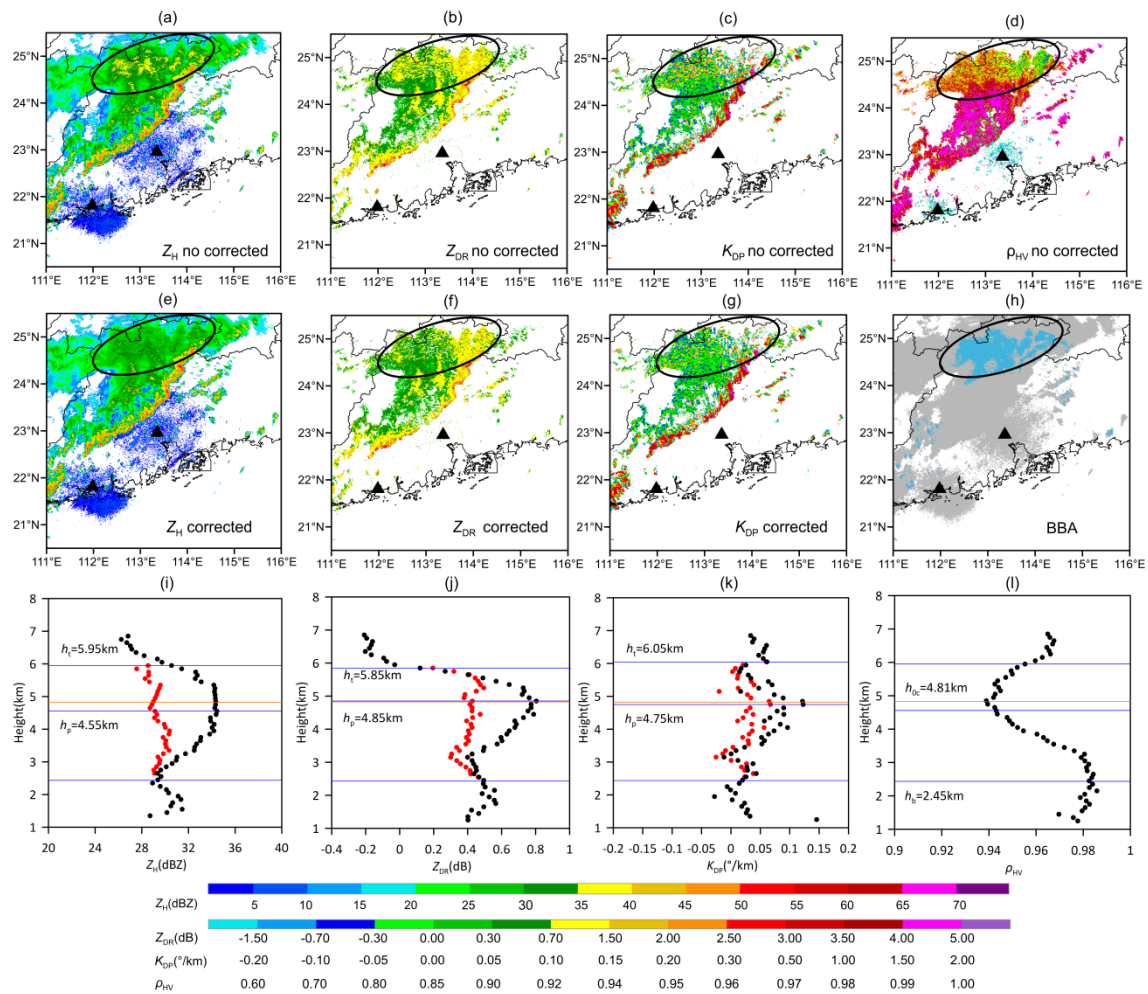


**Figure 10.** The original mosaics for (a)  $Z_H$ , (b)  $Z_{DR}$ , (c)  $K_{DP}$ , and (d)  $\rho_{HV}$  at 20:54 UTC on 15 June, 2016. The corrected mosaics for (e)  $Z_H$ , (f)  $Z_{DR}$ , and (g)  $K_{DP}$  are also shown, respectively. The mosaic data are from the lowest hybrid scans in original polar coordinates. The colors in (h) represent BBA (blue) and non-BBA (gray). The triangles indicate radars. The black circles in (a–h) indicate the main areas that are affected by BB. The AVPDs of (i)  $Z_H$ , (j)  $Z_{DR}$ , (k)  $K_{DP}$ , and (l)  $\rho_{HV}$ , as derived from Guangzhou radar, are also shown. Black dots indicate the original observations, and red dots indicate the corrected values. The corresponding feature heights are marked in the figures.

The BBA mainly falls within the detective range of the Guangzhou radar. The AVPDs of  $Z_H$ ,  $Z_{DR}$ ,  $K_{DP}$ , and  $\rho_{HV}$ , as derived from the Guangzhou radar, are shown in Figure 10. Black dots indicate original observations and red dots indicate corrected values. It can be seen that the original values of  $Z_H$ ,  $Z_{DR}$ , and  $K_{DP}$  show obvious enlargement at a height of around 5 km. The thickness of the BB is larger than the true value due to the beam broadening effect, especially at the BB top height, which may deviate from the true value. However, it does not affect the correction of polarimetric radar data. The large values of the original data at around 5 km become close to the ground data values after correction. However, the discontinuity of the original  $K_{DP}$  vertical profile leads to discontinuity in the corrected  $K_{DP}$  vertical profile. BB correction for  $Z_H$  and  $Z_{DR}$  performs better than that for  $K_{DP}$ . Although the AVPD frequency distribution of  $K_{DP}$  follows the ideal AVPD model, certain vertical profiles of  $K_{DP}$  sometimes cannot follow the ideal AVPD model well; this is why the BB correction performance of  $K_{DP}$  is not very good. This also influences the performances of estimators using the corrected  $K_{DP}$  (Table 3). Therefore,  $K_{DP}$  should not be used to estimate precipitation in the BBA even after correction.

BB correction mitigates the increase of observed data due to the melting of ice particles and can therefore improve QPE performances. However, it is impossible to tell whether this will mitigate the overestimation or underestimation of precipitation, since  $Z_H$  is positively correlated with  $R$

while  $Z_{DR}$  is negatively correlated with  $R$  in the rainfall estimators.  $Z_H$  and  $Z_{DR}$  in BB both increase before correction, but the change of  $R$  is related to the proportion of the two parameters used to estimate precipitation and the contributions of the two parameters to  $R$ . The QPE performances in the BBA are further analyzed in Section 3.3.

### 3.2. Results of the Polarimetric Radar Data Mosaic

On the hypothesis that echoes produced by precipitation exist in each altitude layer and that there is no noise signal, the ideal mosaic heights of the Guangzhou and Yangjiang radars are shown in Figure 11. Some radial vacancies occur around the radar due to beam blockages for lower tilts at these azimuthal angles. In the hybrid scan strategy, the data from the lower tilt are replaced by those from the upper tilt. Their height differences result in radial vacancies. In the overlap area of the two radars, most mosaic height data are also calculated by the data mosaic formula (13); however, the severe beam blockages of the Yangjiang radar lead to a few irregular heights in this area.

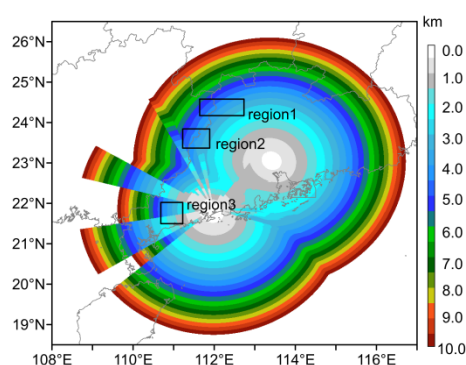


**Figure 11.** The ideal mosaic height. Three areas marked by boxes. Regions 1, 2, and 3 are mainly located at 3–5 km height, and are easily affected by BB.

The mosaic  $Z_H$ ,  $Z_{DR}$ ,  $K_{DP}$ , and  $\rho_{HV}$  are obtained via the proposed mosaic algorithm using the data observed by the Guangzhou and Yangjiang radars at 5:00 on 20 May 2016. The mosaic data and their corresponding  $RQIs$  are shown in Figure 12.

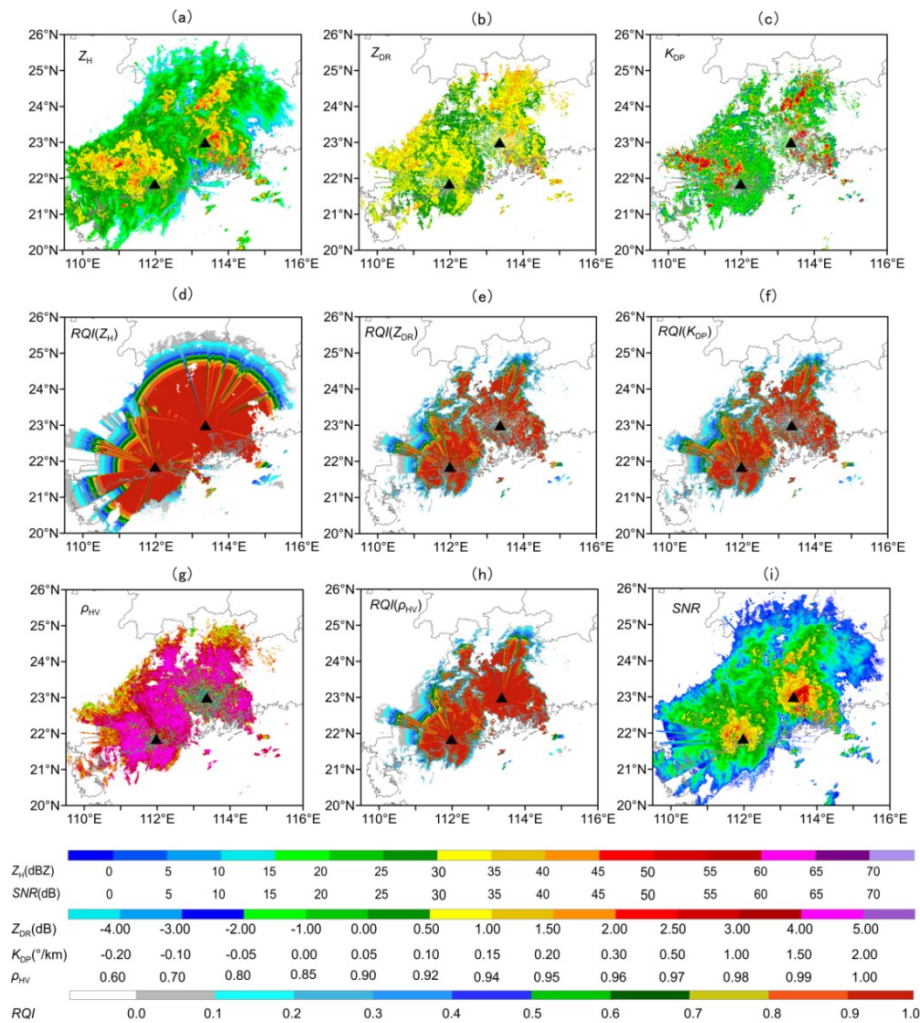


**Figure 12.** Mosaics for (a)  $Z_H$ , (b)  $Z_{DR}$ , (c)  $K_{DP}$ , (g)  $\rho_{HV}$ , and (i) SNR at 5:00 UTC on 20 May 2016. The corresponding RQIs of (d)  $Z_H$ , (e)  $Z_{DR}$ , (f)  $K_{DP}$ , and (h)  $\rho_{HV}$  are also shown next to the radar data. The triangles indicate radars.

All RQI data are distributed with echoes and are larger than zero only where echoes exist. The size of the  $RQI(Z_H)$  with a high value (e.g.,  $>0.9$ ) is the largest. It is mainly influenced by the height of the radar data, since when the height is larger than a given value,  $RQI_{\text{hgt}}$  decreases rapidly. The distributions of  $RQI(Z_{DR})$  and  $RQI(K_{DP})$  behave similarly. The only difference between them is  $RQI_{\text{hgt}}$  because of the different BB correction performances. The distributions of  $RQI(Z_{DR})$ ,  $RQI(K_{DP})$ , and  $RQI(\rho_{HV})$  are all seriously influenced by SNR. The ranges of  $RQI(Z_{DR})$ ,  $RQI(K_{DP})$ , and  $RQI(\rho_{HV})$  are almost the same as the range of SNR larger than 20 dB (shown in Figure 12i). In addition,  $RQI(Z_{DR})$  and  $RQI(K_{DP})$  are also influenced by  $\rho_{HV}$ . Although the SNR is large in areas near the two radars,  $RQI(Z_{DR})$  and  $RQI(K_{DP})$  are small because of the small value of  $\rho_{HV}$ , which corresponds to ground clutter.

Only in the area where  $RQI(Z_{DR})$  and  $RQI(K_{DP})$  are larger than zero do  $Z_{DR}$  and  $K_{DP}$  have a chance to participate in estimating precipitation alongside  $Z_H$ . In the other areas,  $Z_H$  is the only reliable estimation parameter, especially in areas where  $RQI(Z_H)$  is larger than 0.9. It seems that the red areas of  $RQI(Z_H)$  can indicate effective QPE areas, and this will be analyzed via the QPE performance in Section 4.2.

### 3.3. Results of Polarimetric Radar Mosaic QPE

The radar mosaic data are obtained from the nine rainfall events listed in Table 2, and used to estimate precipitation based on the mosaic QPE algorithm proposed in this study. QPE (spatial resolution:  $1 \text{ km} \times 1 \text{ km}$ ) is computed in the detective range of the two radars, but it is evaluated

limited in the common region of the two radars. In order to see the QPE performances on a large scale, especially the performance in the radar beam blocked area, they are evaluated with rain gauge data from within 300 km of each radar. The size of this evaluation region is about 169,821 km<sup>2</sup>. The rainfall accumulations measured at the rain gauge station are used as “true” accumulations. The rainfall accumulations from the radars are accumulated by using the data of every volume scan period on the assumption that the rain rate for the duration of the volume scan is continuous. The average radar-estimated precipitation of the nine grids nearest the rain gauge station is used to evaluate the QPE performance. Since the minimum rainfall measurement of the rain gauge is 0.1 mm, only rainfall measurements exceeding this value were used for evaluation. There are 51,985 sample pairs of QPE-gauge data used for evaluation in this region. The distributions of the *bias ratios* derived from the evaluation results of radar mosaic QPE and the two-radar QPE are shown in Figure 13.

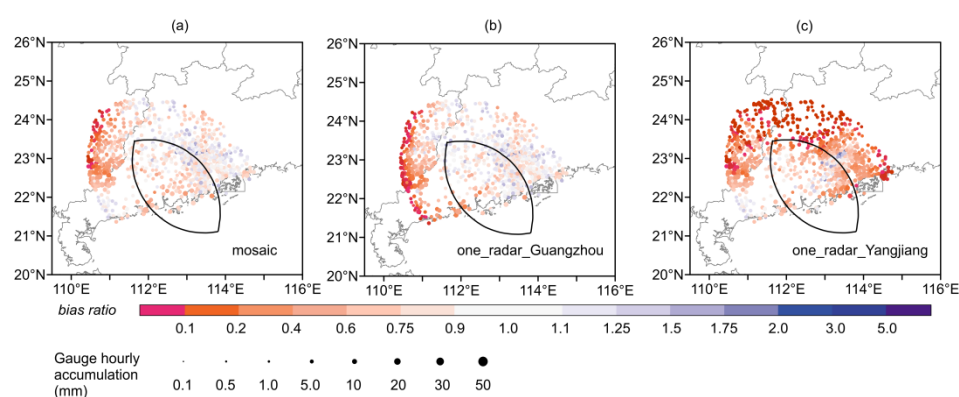


**Figure 13.** *Bias ratio* distributions of (a) radar mosaic QPE and (b,c) two single radars' QPEs. A gauge corresponds to a *bias ratio* value. The bias ratio is computed with the pairs of radar-estimated precipitation and gauge-observed precipitation of this gauge. The evaluation area is less than 300 km from the two radars, and the evaluation results are based on all nine rainfall events. Bubbles indicate the *bias ratio* at the gauge stations. Different colors indicate different *bias ratio* values. Red indicates underestimation and purple indicates overestimation. Bubble size indicates the average hourly rainfall accumulation at each gauge. The inner distance of the spindle shape marked with a black line is less than 180 km from either radar.

Due to the partial beam blockages caused by the complex terrain, the Yangjiang radar QPE is significantly underestimated in the beam blockage directions, and only achieves good estimation performance in a small area close to the radar (Figure 13c). Since the western part of the evaluation area is far from the radar, the beam axis height of the Guangzhou radar is very high when observing this area, such that the beam may overshoot the echo top or only a weak echo can be observed. This leads to clear underestimation of Guangzhou radar QPE in the western evaluation area (Figure 13b). The radar mosaic QPE products take advantage of the QPE products of both radars. Not only does this avoid severe underestimation of Yangjiang radar QPE in partial beam blockages areas, it also avoids underestimation caused by the beam overshooting the echo top far from the Guangzhou radar. This indicates the advantage of the radar mosaic (Figure 13a).

The *bias ratio* distributions clearly show that the radar mosaic can effectively mitigate errors caused by partial beam blockages and the beam partially overshooting cloud tops when using single radar. To quantitatively analyze the other advantages of radar mosaic QPE, only data from rain gauge stations within 180 km of each radar which are in the inner region of the black spindle shape (Figure 13) are selected to calculate the evaluated statistical scores of the radar mosaic and the two single radar QPEs. The size of this evaluation region is about 36,251 km<sup>2</sup>. There are 12,694 sample pairs of QPE-gauge data used for evaluation in this region. The scores are listed in the Table 4. Although the *NB* of the radar mosaic QPE is not very good, it still falls within acceptable limits. The QPE performance of the radar mosaic is better than those of either single radar in terms of *CC*, *RMSE*, and *NE*. After the radar mosaic is constructed, the *RMSE* and *NE* of QPE are reduced by at



least 5.29% and 5.59%, respectively. The main advantage of radar mosaic is that it can improve QPE performances in the blocked area and the area far from the radars compared to the single radar. However, without considering the error caused by partial beam blockages and the beam partially overshooting cloud top, the performance of polarimetric radar mosaic QPE is still better than that of single polarimetric radar QPE. This indicates that the polarimetric radar mosaic QPE algorithm proposed in this study can take advantage of all radars to obtain mosaic data which can be better used to estimate the ground precipitation.

**Table 4.** Evaluated statistical scores of radar mosaic QPE, as well as those of the two single radars.

Method	CC	RMSE (mm)	NE (%)	NB (%)
Radar mosaic QPE	0.86	3.76	39.72	−5.89
Guangzhou Radar QPE	0.85	3.97	42.07	−2.06
Yangjiang Radar QPE	0.65	5.88	64.26	−29.30

In order to know the performance of the radar mosaic QPE in real time, a near real-time statistics of RMSEs derived from the nine rainfall events are shown in Figure 14. RMSEs derived from radar mosaic QPE are smaller than the other two kinds of RMSEs at most time. CCs, NEs, and NBs are not shown here. These three statistical indicators derived from Yangjiang radar QPE are still worst at most time because of the obvious beam blockage. These three statistical indicators derived from radar mosaic QPE and Guangzhou radar QPE performs similar, but radar mosaic QPE performs a little better than Guangzhou radar at most time. These indicate there is a near real-time improvement when the radar mosaic QPE algorithm is applied. This is important for the operational application of the radar mosaic QPE algorithm.

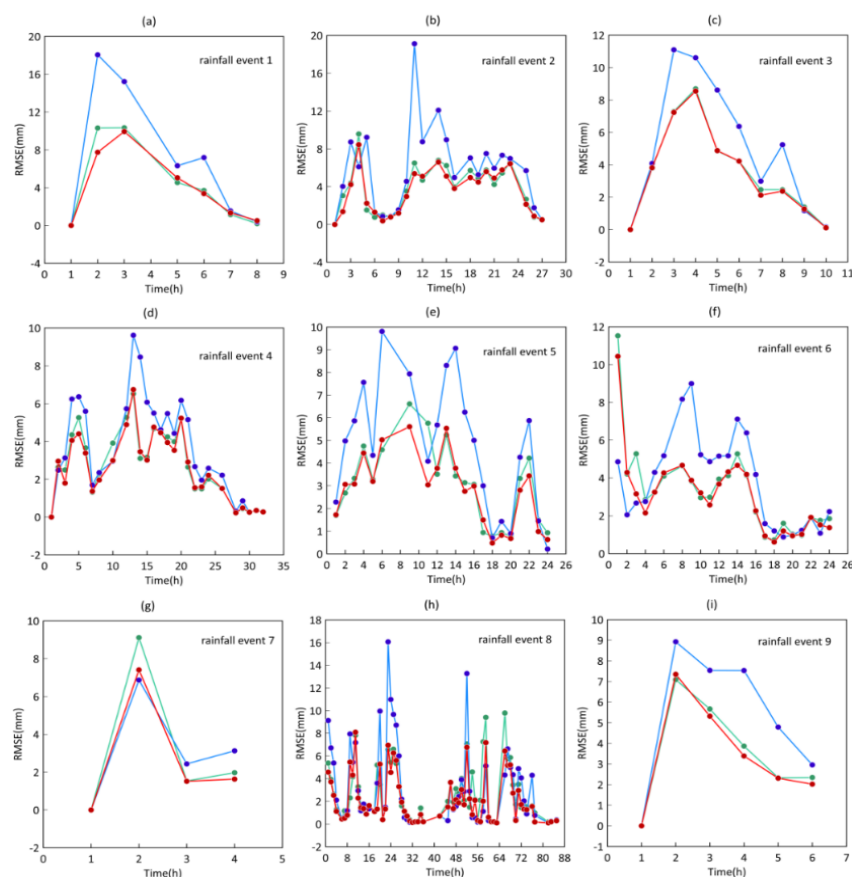


**Figure 14.** (a–i) Time series of RMSEs derived from the nine rainfall events. QPE is also evaluated in the area less than 180 km from either radar. Green, blue, and red lines represent RMSEs derived from Guangzhou radar QPE, Yangjiang radar QPE, and radar mosaic QPE, respectively.

In addition, BB correction is applied to  $Z_H$ ,  $Z_{DR}$ , and  $K_{DP}$  in the polarimetric radar mosaic QPE algorithm. In order to analyze the effect of BB correction upon QPE, the algorithm without BB correction and the algorithm proposed in this study are respectively used to estimate precipitation. The evaluation results are shown in Figure 15.

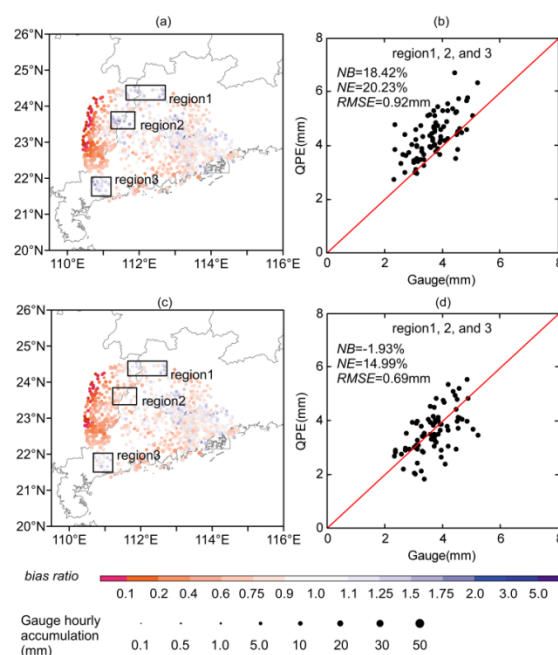


**Figure 15.** Bias ratio distributions of the QPEs estimated by the algorithm without (a) and with (c) BB correction. The color bubbles are the same as those in Figure 13. The associated scatterplots of the QPEs before (b) and after (d) improvements vs. gauge data in regions 1, 2, and 3 are also shown.

The heights of regions 1, 2, and 3 in Figure 15 are about 3–5 km from the mosaic height map shown in Figure 11. The data at these heights are always influenced by BB during May to June in Guangdong province. From the evaluation results, it can be seen that the original polarimetric radar QPE algorithm with  $Z_H$  and  $Z_{DR}$  still overestimates precipitation in the BBA. BB is known to lead to a significant increase in  $Z_H$  and  $Z_{DR}$ . Although the increase in  $Z_{DR}$  can reduce the QPE value, the overestimated results indicate that the increase of  $Z_H$  has a larger effect upon QPE than does the increase of  $Z_{DR}$ . According to the statistics, the percentage of precipitation estimated from  $Z_H$ ,  $Z_H + Z_{DR}$ ,  $K_{DP}$ , and  $K_{DP} + Z_{DR}$  are 90.45%, 7.92%, 0.29%, and 1.34%, respectively. This indicates the RQI of  $Z_H$  is better than  $Z_{DR}$  and  $K_{DP}$ , and the rainfall estimators use  $Z_H$  more often than they use  $Z_{DR}$ . Therefore, the algorithm without BB correction still overestimates precipitation in BBA.

The QPE performances of the two algorithms in regions 1, 2, and 3 are evaluated, and the results are shown in Figure 15b,e. The overestimation in these regions has been mitigated as a result of BB correction. After BB correction, NB is reduced from 18.42% to −1.93%. NE and RMSE are also clearly improved, indicating a reduction in absolute error. These results all indicate that BB correction improves the QPE performances in the BBA.

### 3.4. Sensitivity Tests about the Precipitation Types

The percentages of stratiform precipitation and convective precipitation of these nine rainfall events are 77.60% and 22.40%, respectively. Different percentage of the precipitation types may bring different QPE performances even using the same QPE algorithm. If the precipitation types percentage of these nine rainfall events changes, how the QPE performances would change. In order to solve this question, the influences on QPE caused by percentages of the precipitation types are necessary to be studied.

Some sensitivity tests are performed to see how the evaluated statistics (RMSE, NE, NB) would vary with changing percentages of stratiform and convective. The precipitation in these tests is only

mixed with convective precipitation and stratiform precipitation. The pairs of QPE and gauge data are collected from the nine rainfall events and in the area less than 180 km from either radar. They are divided into two groups according to the precipitation types. One is the convective precipitation group, and the other one is the stratiform precipitation group. Two thousand pairs of the QPE and gauge data are selected for one percentage of the precipitation type. For example, if the convective precipitation percentage is 30%, there would be 600 pairs of the QPE and gauge data that are selected from the convective precipitation group at random. There would be 1400 pairs of the QPE and gauge data that are selected from the stratiform precipitation group at random. There are 11 tests with 11 groups of 2000 pairs of QPE and gauge data corresponding to different percentage of precipitation types. The percentages of convective precipitation data are set at 0%, 10%, 20%, 30%, 40%, 50%, 60%, 70%, 80%, 90%, and 100%, respectively, in the 11 tests. There are 11 groups of the evaluated statistics calculated with the 11 groups of datasets.

The results are shown in Figure 16. *RMSE* changes obviously as the percentage of convective precipitation changes. This is because *RMSE* is influenced by the rain rate. This feature can be seen from Equation (17). As the percentage of convective precipitation becomes large, the rain rate becomes large and so does *RMSE*. *RMSE* ranges from 2.11 mm to 7.34 mm. *NE* and *NB* have nothing to do with the rain rate according to Equations (18) and (19), because they are the relative parameters. There are only three tests, in which *NE* is over 40%. The percentage of convective precipitation is low in these three tests. The worst *NB* appeared in the first test, in which there is no convective precipitation. These indicate the algorithm proposed in this study is a little less effective in estimating the stratiform precipitation than convective precipitation. However, the values of *NE* and *NB* are basically stable in the all 11 tests. *NE* ranges from 35.25% to 45.83%, and *NB* ranges from −9.91% to −6.46%. The values of them are acceptable. These results indicate the radar mosaic QPE algorithm proposed in this study can perform well and stably for any type of precipitation occurred in warm seasons.

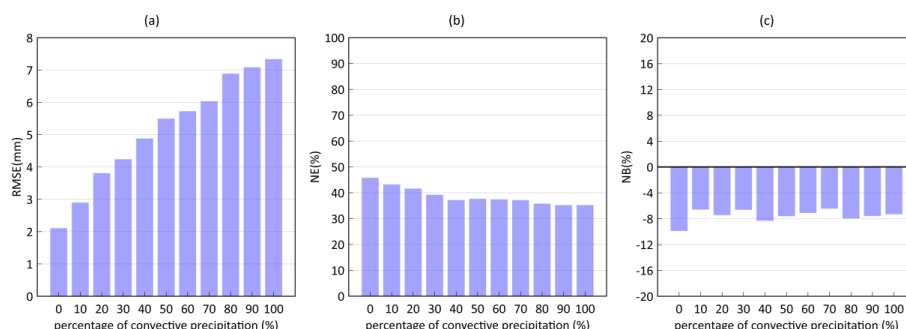


**Figure 16.** (a) *RMSEs*, (b) *NEs*, and (c) *NBs* changing with the percentage of convective precipitation. The precipitation in these tests is only mixed with convective precipitation and stratiform precipitation. The percentages of stratiform precipitation are from 100% to 0% from left to right.

## 4. Discussion

### 4.1. AVPD under BB

BB correction in this study clearly mitigates the increasing effect of  $Z_H$  and  $Z_{DR}$  caused by melting ice particles, causing the average values of  $Z_H$  and  $Z_{DR}$  in BB to approach those under the bottom of the BB. Therefore, the QPE bias in the BBA for all nine rainfall events becomes small, as described in Section 3.3. However, some phenomena still require examination, including the changing trend of data under BB, because they may exert obvious influences upon QPE performance.

Some AVPDs are shown in Figure 17. The green lines represent the changing trends of the  $Z_H$  and  $Z_{DR}$  profiles under BB. The green lines in Figure 17a,d are perpendicular to the horizontal axis, meaning that the averages of  $Z_H$  and  $Z_{DR}$  are basically unchanged with height under the BB. In general, the profiles of  $Z_H$  and  $Z_{DR}$  are basically unchanged under BB, or at least have no discernible



tendency to change. However, significant changes sometimes occur in the profiles of  $Z_H$  and  $Z_{DR}$  under BB, as shown in Figure 17b,c,e,f. These always cause some uncertainties in precipitation estimation.

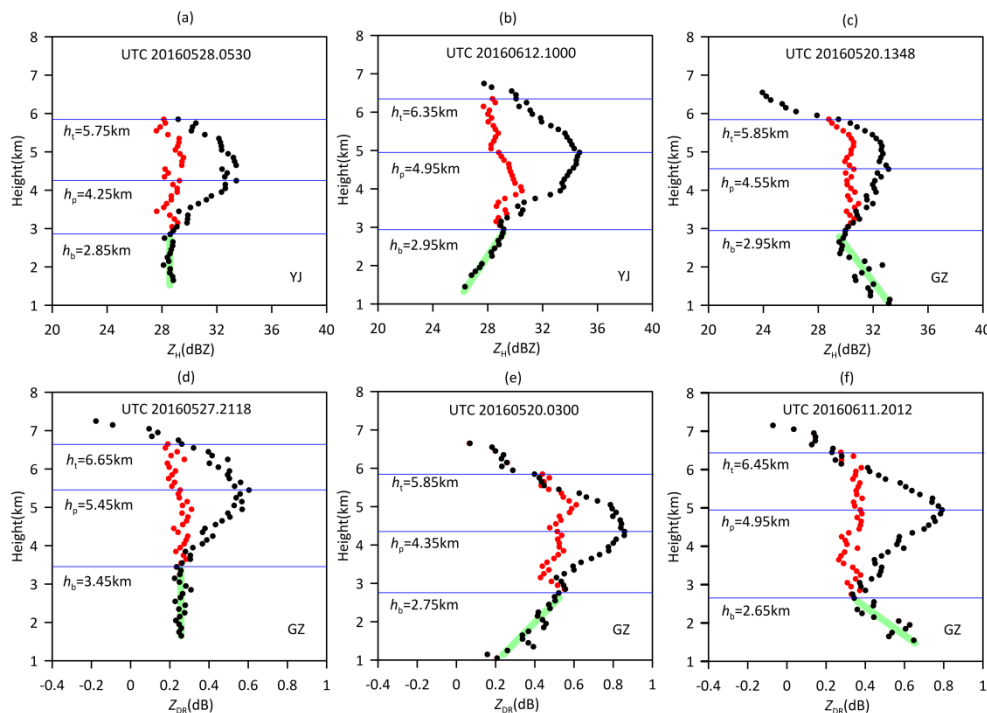


**Figure 17.** AVPDs of (a–c)  $Z_H$  and (d–f)  $Z_{DR}$ . Black dots indicate the original observations and red dots indicate the corrected values. Green lines represent the changing trends of the  $Z_H$  and  $Z_{DR}$  profiles under BB. The corresponding times and feature heights are marked in the figures. “GZ” means data are derived from the Guangzhou radar, and “YJ” means data are derived from the Yangjiang radar.

One trend is that average values decrease along as the height decreases, as shown for  $Z_H$  and  $Z_{DR}$  in Figure 17b,e, respectively. The changing rates under BB differ from those between the BB peak and bottom heights. This indicates that their changing mechanisms are different. The other changing trend is that the average values increase as the height decreases, as shown for  $Z_H$  and  $Z_{DR}$  in Figure 17c,f, respectively. The changing trends under BB are complex and their mechanisms are not clear. The precipitation particles change from the ice phase to the liquid phase in BB. The changing trends under BB are probably associated with changing drop size distribution (DSD). It is necessary to study the vertical change of DSD under BB in future work. This study can also be extended to different precipitation regions and different precipitation types to analyze the vertical changes in DSD and polarimetric parameters to obtain more accurate QPE.

#### 4.2. The Relationship between QPE Accuracy and RQI

RQI in this study can represent the influences of the partial beam blockages, BB, BB correction performance, SNR, and the non-precipitation echoes upon polarimetric radar data. In theory, the RQI value can reflect the accuracy of QPE under the above factors. In the Z11 study, the RQI that only reflected the partial beam blockages and BB showed a good correlation with QPE accuracy. This conclusion is also verified by the study of Chen et al. [39]. However, these studies differed from the present one, in that they used only  $Z_H$  to estimate precipitation, while more polarimetric parameters are used in this study and more factors are considered in our RQI. To study the relationship between QPE accuracy and RQI, the bias ratio and average RQIs of  $Z_H$ ,  $Z_{DR}$ , and  $K_{DP}$  for the nine rainfall events are shown in Figure 18.

The distribution of the average  $RQI$  of  $K_{DP}$  is almost the same as that of  $Z_{DR}$ , because their values only differ in terms of the BB correction performances, and this difference is very small on average. The average  $RQI$  distributions of  $Z_H$ ,  $Z_{DR}$ , and  $K_{DP}$  show some similar characteristics. Their shapes with colors are all limited by the partial beam blockages and the distance from the radars. The average  $RQI$  values of  $Z_H$  are larger than those of  $Z_{DR}$  and  $K_{DP}$ . This is because the low  $SNR$  and  $\rho_{HV}$  decrease the  $RQI$ s of  $Z_{DR}$  and  $K_{DP}$  but have little influence upon the  $RQI$  of  $Z_H$ .

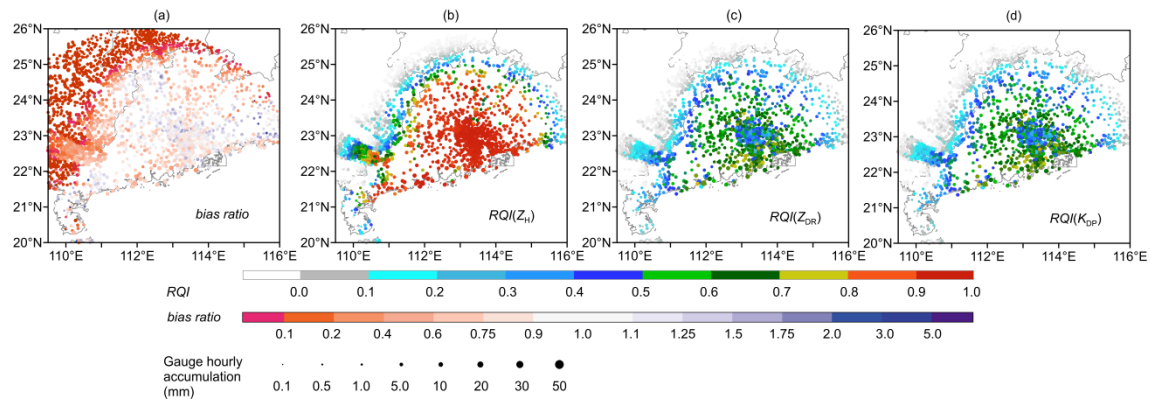


**Figure 18.** (a) Bias ratio distribution of the radar mosaic QPE within almost the entire range that can be detected by the two radars. The color bubbles in (a) are the same as those in Figure 13. (b–d) present the area distributions of the average  $RQI$  of  $Z_H$ ,  $Z_{DR}$ , and  $K_{DP}$ , as derived from nine rainfall events. The color bubbles in (b–d) indicate the average values of  $RQI$  at the gauge stations. Different colors indicate different  $RQI$  values. The bubble size indicates the average hourly rainfall accumulation at each gauge.

A good correlation can be seen between the QPE accuracy and the  $RQI$  of  $Z_H$  from the distributions in Figure 18, as well as the  $RQI$ s of  $Z_{DR}$  and  $K_{DP}$ , despite the values of  $Z_H$  and  $Z_{DR}$  (or  $K_{DP}$ ) being so different. To quantify their correlation, a new bias ratio is proposed, which is shown as follows:

$$\text{new bias ratio} = \begin{cases} \text{bias ratio} & \text{bias ratio} \leq 1 \\ \frac{1}{\text{bias ratio}} & \text{bias ratio} > 1 \end{cases} \quad (21)$$

The CC between the new bias ratio and the average  $RQI$  of  $Z_H$  ( $Z_{DR}$  and  $K_{DP}$ ) is 0.80 (0.71 and 0.70). This quantitatively verifies the view that there is good correlation between the QPE accuracy and the  $RQI$  of  $Z_H$  ( $Z_{DR}$  and  $K_{DP}$ ). Such correlation exists because the  $RQI$  partially models the uncertainties due to the partial beam blockages, BB, BB correction performance,  $SNR$ , and the non-precipitation echoes. However, the uncertainties associated with spatially varying drop size distributions still affect the correlation between QPE accuracy and the  $RQI$  of  $Z_H$  ( $Z_{DR}$  and  $K_{DP}$ ), because  $RQI$  cannot represent these uncertainties. Based on the good correlation found between QPE accuracy and the  $RQI$  of  $Z_H$ , an effective QPE area can be defined with an  $RQI$  of  $Z_H$  larger than 0.9. QPE performances are evaluated within the radars' detection range. At the same time, only the QPEs corresponding to the  $RQI$ s of  $Z_H$  larger than 0.9 are used for evaluation, and the performance is basically acceptable in terms of CC (0.83), RMSE (4.00 mm), NE (44.8%), and NB (−2.84%). Therefore, the effective QPE area defined here is reasonable. This area can help in obtaining accurate radar QPE information, which will be beneficial to the application of radar QPE products. Besides this, since there is good correlation between the QPE accuracy and the  $RQI$ ,  $RQI$  can reflect the QPE accuracy to some extent. Therefore,  $RQI$  can be used in a weigh function when radar QPE is merged with other precipitation products derived from other different sensors. This is also beneficial to the application of radar QPE products.

## 5. Conclusions

A new polarimetric radar mosaic QPE algorithm based on  $RQI$  was proposed. This algorithm can be used in different regions with the default values adjusted according to the characteristics of local radar.  $RQI$  of this algorithm can quantitatively describe the quality of  $Z_H$ ,  $Z_{DR}$ ,  $K_{DP}$ , and  $\rho_{HV}$ , and is used in high-quality data screening and mosaic data merging. In this algorithm, BB correction is performed to mitigate the increase of  $Z_H$ ,  $Z_{DR}$ , and  $K_{DP}$  caused by the melting ice particles in the rainfall events of warm seasons. The new algorithm is evaluated based on nine rainfall events occurring in Guangdong province, China, and detected by the Guangzhou and Yangjiang polarimetric radars. Main conclusions are summarized as follows:

1. After BB correction, the values of  $Z_H$ ,  $Z_{DR}$ , and  $K_{DP}$  in BB become closer to those under BB than before. However, the BB correction performance of  $K_{DP}$  is not as good as that of  $Z_H$  and  $Z_{DR}$ . Only the corrected  $Z_H$  and  $Z_{DR}$  are used to estimate precipitation in the BBA. Precipitation is overestimated even when using polarimetric parameters in the BBA prior to BB correction. BB correction in this new radar mosaic QPE algorithm obviously mitigates the overestimation of rainfall in the BBA.
2. The new polarimetric radar mosaic QPE algorithm based on  $RQI$  can combine the different radars' advantages to improve QPE performances in the blocked area and the area far from the radars, thereby obtaining more accurate and wider range of mosaic data and QPE products. The new algorithm also performs better than the single radar QPE algorithm in the area close to the two radars. Within 180 km of the radars, the  $RMSE$  and  $NE$  decrease by at least 5.29% and 5.59%, respectively. The near real-time statistics of evaluated indicators show that there is a near real-time improvement when the radar mosaic QPE algorithm is applied. It is important for the operational application of this new algorithm.
3. The sensitivity tests with the changing percentage of stratiform and convective precipitation show that  $NE$  and  $NB$  are basically stable when this percentage changes. The new polarimetric radar mosaic QPE algorithm can perform well and stably for any type of precipitation occurred in warm seasons.
4. There is good correlation between QPE accuracy and the  $RQI$  of  $Z_H$  ( $Z_{DR}$  and  $K_{DP}$ ). An effective QPE area can be defined with an  $RQI$  of  $Z_H$  larger than 0.9, resulting in a small bias ( $NB = -2.84\%$ ) for rainfall events in this study.

This study has presented the advantages of our proposed polarimetric radar mosaic QPE algorithm; however, only two polarimetric radars have been considered because of the limitations of data collection. In fact, since more polarimetric radars data being mosaicked together would have the benefit of more high-quality data, they would be able to obtain better QPE products. Moreover,  $RQI$  can also represent the polarimetric radar data quality, meaning this new polarimetric radar mosaic QPE algorithm can be applied to polarimetric radars of different quality. It has great potential applications to operational work; therefore, our new algorithm is expected to be used to evaluate the operational performances of more operational polarimetric radars in future studies. Although the algorithm presented here is designed for polarimetric radars in China, it may also serve as a reference for polarimetric radar mosaicking in other countries.

**Author Contributions:** Conceptualization, Y.Z. and L.L.; methodology, Y.Z. and L.L.; software, Y.Z.; validation, Y.Z., L.L., and H.W.; formal analysis, L.L.; investigation, Y.Z.; resources, H.W.; data curation, H.W.; writing—original draft preparation, Y.Z.; writing—review and editing, Y.Z., L.L., and H.W.; visualization, Y.Z.; supervision, L.L.; project administration, Y.Z.; funding acquisition, Y.Z. and L.L. All authors have read and agreed to the published version of the manuscript.

**Funding:** This research was jointly funded by the National Natural Science Foundation of China (41875036), Basic Research Fund of CAMS (2020Y017), and Scientific Research Projects of CAMS (2019Z002).

**Conflicts of Interest:** The authors declare no conflict of interest.

## References

1. Bringi, V.N.; Chandrasekar, V. *Polarimetric Doppler Weather Radar: Principles and Applications*; Cambridge University Press: Cambridge, UK, 2001; ISBN 1139429469.
2. Chen, H.; Chandrasekar, V.; Tan, H.; Cifelli, R. Rainfall estimation from ground radar and TRMM Precipitation Radar using hybrid deep neural networks. *Geophys. Res. Lett.* **2019**, *46*, 10669–10678, doi:10.1029/2019GL084771.
3. Zhang, J.; Tang, L.; Cocks, S.; Zhang, P.; Ryzhkov, A.; Howard, K.; Langston, C.; Kaney, B. A Dual-polarization Radar Synthetic QPE for Operations. *J. Hydrometeorol.* **2020**, doi:10.1175/JHM-D-19-0194.1.
4. Wen, Y.; Kirstetter, P.; Hong, Y.; Gourley, J.J.; Xue, X. Evaluation of a method to enhance real-time, ground radar-based rainfall estimates using climatological profiles of reflectivity from space. *J. Hydrometeorol.* **2016**, *17*, 761–775, doi:10.1175/JHM-D-15-0062.1.
5. Zhang, J.; Howard, K.; Gourley, J.J. Constructing Three-Dimensional Multiple-Radar Reflectivity Mosaics: Examples of Convective Storms and Stratiform Rain Echoes. *J. Atmos. Ocean. Technol.* **2005**, *22*, 30–42, doi:10.1175/JTECH-1689.1.
6. Zhang, J.; Howard, K.; Langston, C.; Vasiloff, S.; Kaney, B.; Arthur, A.; Cooten, S.V.; Kelleher, K.; Kitzmiller, D.; Ding, F.; et al. National mosaic and multi-sensor QPE (NMQ) system: Description, results, and future plans. *Bull. Am. Meteorol. Soc.* **2011**, *92*, 1321–1338, doi:10.1175/2011BAMS-D-11-00047.1.
7. Xiao, Y.; Liu, L.; Yang, H. Technique for generating hybrid reflectivity field based on 3D mosaicked reflectivity of weather radar network. *Act. Meteor. Sin.* **2008**, *66*, 470–473, doi:10.3724/SP.J.1047.2008.00014. (In Chinese)
8. Gao, X.; Liang, J.; Li, C. Radar quantitative precipitation estimation techniques and effect evaluation. *J. Trop. Meteor.* **2012**, *28*, 77–88, doi:10.1007/s11783-011-0280-z. (In Chinese)
9. Gou, Y.; Liu, L.; Yang, J.; Wu, C. Operational application and evaluation of the quantitative precipitation estimates algorithm based on the multi-radar mosaic. *Act. Meteor. Sin.* **2014**, *72*, 731–748, doi:10.11676/qxxb2014.050. (In Chinese).
10. Chu, Z.; Ma, Y.; Zhang, G.; Wang, Z.; Han, J.; Kou, L.; Li, N. Mitigating Spatial Discontinuity of Multi-Radar QPE Based on GPM/KuPR. *Hydrology* **2018**, *5*, 48, doi:10.3390/hydrology5030048.
11. Zhang, J.; Howard, K.; Langston, C.; Kaney, B.; Qi, Y.; Tang, L.; Grams, H.; Wang, Y.; Cocks, S.; Martinaitis, S.; et al. Multi-Radar Multi-Sensor (MRMS) Quantitative Precipitation Estimation: Initial Operating Capabilities. *Bull. Am. Meteorol. Soc.* **2016**, *97*, 621–638, doi:10.1175/BAMS-D-14-00174.1.
12. Zhang, Y.; Liu, L.; Wen, H.; Wu, C.; Zhang, Y.H. Evaluation of the Polarimetric-Radar Quantitative Precipitation Estimates of an Extremely Heavy Rainfall Event and Nine Common Rainfall Events in Guangzhou. *Atmosphere* **2018**, *9*, 330, doi:10.3390/atmos9090330.
13. Wang, Y.T.; Chandrasekar, V. Algorithm for estimation of the specific differential phase. *J. Atmos. Ocean. Technol.* **2009**, *26*, 2565–2578, doi:10.1175/2009JTECHA1358.1.
14. Grazioli, J.; Schneebeli, M.; Berne, A. Accuracy of phase-based algorithms for the estimation of the specific differential phase shift using simulated polarimetric weather radar data. *IEEE Geosci. Remote. Sens. Lett.* **2013**, *11*, 763–767, doi:10.1109/LGRS.2013.2278620.
15. Huang, H.; Zhang, G.; Zhao, K.; Giangrande, S.E. A hybrid method to estimate specific differential phase and rainfall with linear programming and physics constraints. *IEEE Trans. Geosci. Remote. Sens.* **2016**, *55*, 96–111, doi:10.1109/TGRS.2016.2596295.
16. Wu, C.; Liu, L.; Wei, M.; Xi, B.; Yu, M. Statistics-based optimization of the polarimetric radar Hydrometeor Classification Algorithm and its application for a squall line in South China. *Adv. Atmos. Sci.* **2018**, *35*, 296–316, doi:10.1007/s00376-017-6241-0.
17. Ryde, J.W. The attenuation and radar echoes produced at centimeter wavelengths by various meteorological phenomena. In *Meteorological Factors in Radio Wave Propagation*, London, U.K.; The Physical Society: London, UK, 1946; pp. 169–188.
18. Austin, P.M.; Bemis, A.C. A Quantitative Study of the 'Bright Band' in Radar Precipitation Echoes. *J. Atmos. Sci.* **1950**, *7*, 145–151, doi:10.1175/1520-0469(1950)007<0145:AQSOTB>2.0.CO;2.
19. Wexler, R.; Atlas, D.; Mason, B.J. Factors influencing radar-echo intensities in the melting layer. *Quart. J. Roy. Meteor. Soc.* **1956**, *82*, 349–351, doi:10.1002/qj.49708235312.

20. Lhermitte, R.M.; Atlas, D. Doppler fall speed and particle growth in stratiform precipitation. In Proceedings of the 10th Conference on Radar Meteorology, Washington, DC, USA, 22–25 April 1963; American Meteorological Society: Washington, DC, USA, 1963; pp. 297–302.
21. Zhang, J.; Langston, C.; Howard, K. Brightband Identification Based on Vertical Profiles of Reflectivity from the WSR-88D. *J. Atmos. Ocean. Technol.* **2008**, *25*, 1859–1872, doi:10.1175/2008JTECHA1039.1.
22. Gourley, J.J.; Calvert, C.M. Automated Detection of the Bright Band Using WSR-88D Data. *Wea. Forecast.* **2003**, *18*, 585–599, doi:10.1175/1520-0434(2003)018<0585:ADOTBB>2.0.CO;2.
23. Zhang, J.; Qi, Y. A Real-Time Algorithm for the Correction of Brightband Effects in Radar-Derived QPE. *J. Hydrometeorol.* **2010**, *11*, 1157–1171, doi:10.1175/2010JHM1201.1.
24. Qi, Y.; Zhang, J. Correction of Radar QPE Errors Associated with Low and Partially Observed Brightband Layers. *J. Hydrometeorol.* **2013**, *14*, 1933–1943, doi:10.1175/JHM-D-13-040.1.
25. Rico-Ramirez, M.A.; Cluckie, I.D.; Han, D. Correction of the bright band using dual-polarisation radar. *Atmos. Sci. Lett.* **2005**, *6*, 40–46, doi:10.1002/asl.89.
26. Reino, K.; Laura, C.A.; Jason, S. Estimation of Melting Layer Altitudes from Dual- Polarization Weather Radar Observations. In Proceedings of the Eighth European Conference on Radar in Meteorology and Hydrology, Garmisch-Partenkirchen, Germany, 1–5 September 2014.
27. Mario, M.; Nicoletta, R.; Elisa, A.; Eugenio, G.; Luca, B. Investigation of weather radar quantitative precipitation estimation methodologies in complex orography. *Atmosphere* **2017**, *8*, 34, doi:10.3390/atmos8020034.
28. Friedrich, K.; Hagen, M.; Einfalt, T. A Quality Control Concept for Radar Reflectivity, Polarimetric Parameters, and Doppler Velocity. *J. Atmos. Ocean. Technol.* **2006**, *23*, 865–887, doi:10.1175/JTECH1920.1.
29. Vulpiani, G.; Montopoli, M.; Passeri, L.D.; Gioia, A.G.; Giordano, P.; Marzano, F.S. On the Use of Dual-Polarized C-Band Radar for Operational Rainfall Retrieval in Mountainous Areas. *J. Appl. Meteor. Climatol.* **2012**, *51*, 405–425, doi:10.1175/JAMC-D-10-05024.1.
30. Tabary, P. The New French Operational Radar Rainfall Product. Part I: Methodology. *Wea. Forecast.* **2010**, *22*, 393–408, doi:10.1175/WAF1004.1.
31. Qi, Y.; Zhang, J. A Physically Based Two-Dimensional Seamless Reflectivity Mosaic for Radar QPE in the MRMS System. *J. Hydrometeorol.* **2017**, *18*, 1327–1340, doi:10.1175/JHM-D-16-0197.1.
32. Chen, C.; Hu, Z.; Hu, S.; Zhang, Y. Preliminary analysis of data quality of Guangzhou S-band polarimetric weather radar. *J. Trop. Meteor.* **2018**, *34*, 59–67, doi:1004-4965(2018)01-0059-09. (In Chinese).
33. Bech, J.; Codina, B.; Lorente, J.; Bebbington, D. The sensitivity of single polarization weather radar beam blockage correction to variability in the vertical refractivity gradient. *J. Atmos. Ocean. Technol.* **2003**, *20*, 845–855, doi:10.1175/1520-0426(2003)020<0845:TSOSPW>2.0.CO;2.
34. Wen, H.; Zhang, L.; Liang, H.; Zhang, Y. Radial interference echo identification algorithm based on fuzzy logic for weather radar. *Act. Meteor. Sin.* **2020**, *78*, 116–127, doi:10.11676/qxxb2020.010. (In Chinese)
35. Shi, Z.; Wei, F.; Chandrasekar, V. Radar-based quantitative precipitation estimation for the identification of debris flow occurrence over earthquake-affected regions in Sichuan, China. *Nat. Hazards Earth Syst. Sci.* **2017**, *18*, 765–780, doi:10.5194/nhess-18-765-2018.
36. Qi, Y.; Zhang, J.; Zhang, P.; Cao, Q. VPR correction of bright band effects in radar QPEs using polarimetric radar observations. *J. Geophys. Res.* **2013**, *118*, 3627–3633, doi:10.1002/jgrd.50364.
37. Zhang, J.; Qi, Y.; Langston, C.; Kaney, B. Radar Quality Index (RQI)—a combined measure for beam blockage and VPR effects in a national network. In Proceedings of the Symposium Weather Radar and Hydrology, Exeter, UK, 18–21 April 2011.

38. Wu, C. Data Quality Analysis, Hydrometeor Classification and Mosaic Application of Polarimetric Radars in China. Ph.D. Thesis, Nanjing University of Information Science and Technology, Nanjing, China, 2018.
39. Chen, S.; Gourley, J.J.; Hong, Y.; Kirstetter, P.E.; Zhang, J.; Howard, K.; Flaming, Z.L.; Hu, J.; Qi, Y. Evaluation and uncertainty estimation of NOAA/NSSL next-generation National Mosaic QPE (Q2) over the continental United States. *J. Hydrometeor.* **2013**, *14*, 1308–1322, doi:10.1175/JHM-D-12-0150.1.

**Publisher's Note:** MDPI stays neutral with regard to jurisdictional claims in published maps and institutional affiliations.



© 2020 by the authors. Licensee MDPI, Basel, Switzerland. This article is an open access article distributed under the terms and conditions of the Creative Commons Attribution (CC BY) license (<http://creativecommons.org/licenses/by/4.0/>).